RECLAMATION
Managing Water in the West

User's Manual for SRH-Meander

(Sedimentation and River Hydraulics – Meandering, Version 1.0)

REPORT DOCUMENTATION PAGE

1. REPORT DATE *(DD-MM-YYYY)* 05-01-2007	2. REPORT TYPE Numerical Model Documentation and User's Manual	3. DATES COVERED *(From - To)* 03-01-06-05-01-2007

4. TITLE AND SUBTITLE User's Manual for SRH-M 1.0 (Sedimentation and River Hydraulics – Meandering, Version 1.0)	5a. CONTRACT NUMBER
	5b. GRANT NUMBER
	5c. PROGRAM ELEMENT NUMBER
6. AUTHOR(S) Blair P. Greimann, Ph.D., P.E. Jianchun Victor Huang, Ph.D., P.E. Timothy J. Randle, M.S., P.E.	5d. PROJECT NUMBER
	5e. TASK NUMBER
	5f. WORK UNIT NUMBER

7. PERFORMING ORGANIZATION NAME(S) AND ADDRESS(ES) Sedimentation and River Hydraulics Group, Technical Service Center, Bureau of Reclamation, Denver Federal Center, Bldg. 67, PO BOX 25007 (86-68540), Denver, CO 80225	8. PERFORMING ORGANIZATION REPORT NUMBER
9. SPONSORING/MONITORING AGENCY NAME(S) AND ADDRESS(ES)	10. SPONSOR/MONITOR'S ACRONYM(S)
	11. SPONSOR/MONITOR'S REPORT NUMBER(S)

12. DISTRIBUTION/AVAILABILITY STATEMENT

13. SUPPLEMENTARY NOTES

14. ABSTRACT

SRH-M (Sedimentation and River Hydraulics – Meander) is a computer model that simulates the bed topography, flow field, and bank erosion rate in curved channel with an erodible bed. In each time step, SRH-M first calculates the flow field based on the standard step method or normal depth method. It then computes the channel bank erosion rate. Finally the channel alignment is updated with the erosion rate, followed by the channel cutoff if needed. The model can be used to predict the channel migration in meandering rivers.

15. SUBJECT TERMS
Sediment Transport, Alluvial Rivers, Numerical Modeling, Hydraulic Model

16. SECURITY CLASSIFICATION OF:			17. LIMITATION OF ABSTRACT	18. NUMBER OF PAGES	19a. NAME OF RESPONSIBLE PERSON Blair Greimann
a. REPORT	b. ABSTRACT	a. THIS PAGE			19b. TELEPHONE NUMBER *(Include area code)* *303 445-2563*

User's Manual for SRH-M

(Sedimentation and River Hydraulics – Meandering, Version 1.0)

Prepared by

Blair P. Greimann, Ph.D., P.E.
Jianchun Victor Huang, Ph.D., P.E.
Timothy J. Randle, M.S., P.E.
Sedimentation and River Hydraulic Group

Acknowledgments

Disclaimer

CONTENTS

TABLES

FIGURES

1. INTRODUCTION

1.1 Background

SRH-Meander (Sedimentation and River Hydraulics - Meandering) is a computer model that simulates the bed topography, flow field, and bank erosion rate in a curved channel with an erodible bed. In each time step, SRH-M first calculates the flow field based on the standard step method or normal depth method. It then computes the channel bank erosion rate. Finally the channel alignment is updated with the erosion rate, followed by a channel cutoff if needed. The model can be used to predict the channel migration in meandering rivers.

SRH-Meander is part of the SRH series, developed in the Sedimentation and River Hydraulic Group, Technical Service Center, Bureau of Reclamation. Besides SRH-Meander, currently SRH series also includes SRH-1D (Sedimentation and River Hydraulics – One Dimension) and SRH-W (Sedimentation and River Hydraulics – Watershed).

1.2 Meandering River Description

As the river follows a meander bend, the centrifugal force causes the water surface elevation to be slightly higher on the outside of the bend. This causes a pressure imbalance perpendicular to the main flow direction, which then causes a secondary flow cell. This secondary flow carries fast moving fluid from the upper portion of the flow on the inner bank to the upper portion of flow on the outer bank. Likewise, the lower portion of the flow from the outer bank is transferred to the lower portion of flow of the inner bank. For large radii bends, there is a net transfer of streamwise fluid momentum to the outside of the bank. This transfer of momentum causes the velocity to be larger on the outside of the bend. This process is shown in Figure 1.1 (from Edwards and Smith, 2001). Also, because the higher velocities are on the outside of the bend, the sediment is scoured on the outside of the bend and deposited on the inner portion of the downstream bend.

River migration can be influenced by several factors. The magnitude of the flow

is important in determining the river depth, velocity, and width. The particular sinuosity and meander pattern will control the velocity distribution across the channel. The size of the sediment composing the bank can control its resistance to failure. For fine-grained banks, the cohesive properties can cause the banks to maintain a high degree of strength and the failure mechanisms can be different between cohesive banks and non-cohesive banks. Roots from vegetation can also increase the strength of banks. As trees fall into the river, they can significantly alter the flow pattern and either reduce or increase bank erosion rates. Trees can play an important role in river morphology. The river bed material can also influence the bank erosion rates (Nanson and Hickin, 1986). If river bed material is resistant to erosion and the river has a sediment deficit, the river may pick up sediment from the banks to satisfy that deficit. Conversely, if the banks are resistant to erosion, but the bed erodes easily, bank failure may still occur if the banks are undermined by excessive bed erosion.
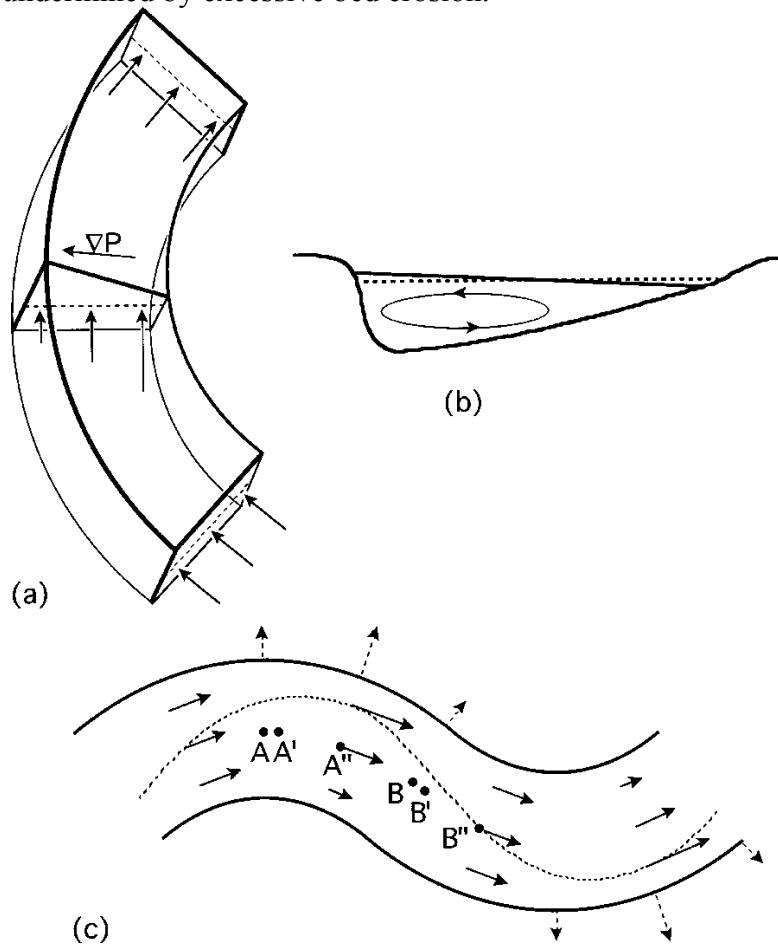
Figure 1.1. Figure showing physical processes in river meanders (from Edwards and Smith, 2001).

The following description of Figure 1.1 is taken from Edwards and Smith (2001):

(a) Three-dimensional view of a river bend to the right, showing the outward hydrostatic pressure gradient ∇P created by the surface elevation gradient, and showing the resulting Bernoulli shear in the downstream velocity (arrows). As fluid elements near the inside bank enter the low-pressure region at the bend apex, their velocities increase by Bernoulli's law. Similarly, the downstream velocities of fluid elements near the outside of the bend decrease as they approach the high-pressure region at the bend apex. This Bernoulli shear straightens small-radius bends by eroding the inside bank.

(b) Vertical cross section through a river bend to the right, as seen by a river-bound observer facing downstream, showing counterclockwise secondary flow and the resulting deepening near the outside ''cut'' bank. This secondary flow convectively transports downstream momentum toward the outside bank, and dominates over Bernoulli shear for large-radius bends, leading to lateral and downstream migration of meander bends.

(c) Schematic downstream velocities (solid arrows) for one cycle of a large wavelength sinusoidal river. Solid traces represent the river banks, whereas the dashed trace represents the locus of maximum velocity, called the thalweg, which lags behind the channel curvature by the decay length D (Eq. 1). Large downstream velocities near a bank increase the local shear and the local bank erosion rates, leading to lateral and downstream migration of the meander pattern (dashed arrows). For typical large-radius bends such as those shown, the secondary flow overwhelms Bernoulli shear, leading to high velocities near the outsides of bends, with the largest velocities and migration rates downstream of the bend apex. For the first (right) bend, points A, A′, and A″ respectively represent the bend apex, the location of strongest secondary flow, and the location of maximum cross-stream shear in the downstream velocity. Also at A″, the thalweg makes its closest approach to the left bank. Points B, B′, and B″ respectively designate an inflection point in the channel curvature, a location of vanishing secondary flow, and a location of vanishing cross-stream shear in the downstream velocity (a meander

''node''). The A–A′ and B–B′ distances, neglected herein, are considerably smaller than D, which scales the A–A″ and B–B″ distances.

1.3 SRH-Meander Capabilities

SRH-Meander is a numerical model developed to simulate channel migration in meandering rivers. Some of the model's capabilities are:

- Computation of water surface profiles in a single channel with standard step method or normal depth method.
- Calculation of bank erosion rate with Randle's minimization method or Johannesson and Parker's linearization method.
- Sixteen different non-cohesive sediment transport equations that are applicable to a wide range of hydraulic and sediment conditions.
- Channel cutoff simulation.
- Computation of channel alignment.
- Computation of river topography.
- GIS input of channel alignment.
- GIS input of channel erosion rate parameters.
- GIS raster file input of river and floodplain elevations.

1.4 Limits of Application

SRH-Meander is an engineering tool for solving channel migration in meandering rivers with the following limitations:

(1) SRH-Meander is a simplified model with minimization method or linearization method. It should only be applied to situations channels with small width and radius ratio.

(2) The erosion rate parameters are highly sensitive to the bed material, vegetation, large woody debris, and other unknown factors, calibration is required in choosing this parameters.

(2) Many of the sediment transport modules and concepts used in SRH-Meander are simplified approximations of real phenomena. Those approximations and their limits of validity are embedded in the model.

(3) SRH-Meander is currently compiled to run only within the Windows 2000/XP operating system.

1.5 Acquiring SRH-Meander

The latest information about SRH-Meander version 1.0 is placed on the Web and can be found by accessing http://www.usbr.gov/pmts/sediment and following the links on the web page. Requests may be sent directly to the Bureau of Reclamation's Sedimentation and River Hydraulics Group (Attention: SRH Model Support, U.S. Bureau of Reclamation, Sedimentation and River Hydraulics Group, P.O. Box 25007 (D-8540), Denver, CO 80225). SRH-Meander is under continuous development and improvement. A user is encouraged to check the SRH-Meander web page regularly for updates.

1.6 Disclaimer

The program SRH-Meander and information in this manual are developed for use at the Bureau of Reclamation. Reclamation does not guarantee the performance of the program, nor help external users solve their problems. Reclamation assumes no responsibility for the correct use of SRH-Meander and makes no warranties concerning the accuracy, completeness, reliability, usability, or suitability for any particular purpose of the software or the information contained in this manual. SRH-Meander is a program that requires engineering expertise to be used correctly. Like other computer programs, SRH-Meander is potentially fallible. All results obtained from the use of the program should be carefully examined by an experienced engineer to determine if they are reasonable and accurate. Reclamation will not be liable for any special, collateral, incidental, or consequential damages in connection with the use of the software.

2. Flow Solution

This chapter describes methods to compute the hydraulic solution in SRH-Meander. SRH-Meander provides two types of flow solutions, the normal depth method and the standard step method.

2.1 Standard Step Method

SRH-Meander uses the standard step method to solve the energy equation for steady gradually varied flows. Presently, only subcritical and critical flow profiles are calculated. The energy equation for steady gradually varied flow between downstream cross section 1 and upstream cross section 2 is expressed as:

$$Z_2 + \beta_2 \frac{V_2^2}{2g} - Z_1 - \beta_1 \frac{V_1^2}{2g} = h_f + h_c \tag{2.1}$$

where: Z_1, Z_2 = water surface elevations at cross sections 1 and 2, respectively;

V_1, V_2 = average velocities at cross sections 1 and 2, respectively;

β_1, β_2 = velocity distribution coefficients at cross sections 1 and 2, respectively;

g = gravitational acceleration;

h_f = friction loss between cross sections 1 and 2, and

h_c = contraction or expansion losses between cross sections 1 and 2.

The equation for friction loss may be calculated in two ways as:

$$h_{fa} = \sqrt{S_{f_1} S_{f_2}} (x_2 - x_1) \tag{2.2}$$

$$h_{fb} = \left[\frac{2Q}{(K_1 + K_2)} \right]^2 (x_2 - x_1) \tag{2.3}$$

where: S_{f_1}, S_{f_2} = friction slopes at cross sections 1 and 2, respectively;

x_1, x_2 = streamwise coordinates of cross sections 1 and 2, respectively;

Q = flow rate; and

K_1, K_2 = conveyance at cross sections 1 and 2, respectively.

The actual friction loss used is the minimum of the two:

$$h_f = \min(h_{fa}, h_{fb})$$ (2.4)

For a specific discharge, the conveyance, K, is used to determine the friction slope in Eq. 2.3:

$$S_f = \left(\frac{Q}{K}\right)^2$$ (2.5)

where K is computed from the Manning's equation:

$$Q = KS_f^{1/2} = \frac{C_m}{n} AR^{2/3} S_f^{1/2}$$ (2.6)

where: n = Manning's coefficient;

A = cross-sectional area;

R = hydraulic radius (A/P);

P = wetted perimeter; and

C_m = 1.486 for English units or 1.0 for SI units.

The equation for contraction or expansion losses is expressed as:

$$h_c = C_c \left| \frac{\beta_1 V_1^2}{2g} - \frac{\beta_2 V_2^2}{2g} \right|$$ (2.7)

where: C_c = a user defined contraction or expansion coefficient.

The expansion coefficient is used when the velocity head at the downstream section 1 is less than that at the upstream section 2. Conversely, the contraction coefficient is used when the velocity head at the downstream section 1 is greater than that at the upstream section 2. This is similar to the way ☰C-RAS (Brunner, 2001) treats energy loss.

Standard step method is used to solve Eq. 2.1, which can be expressed as:

$$f(Z_2) = Z_2 + \beta_2 \frac{V_2^2}{2g} - Z_1 - \beta_1 \frac{V_1^2}{2g} - h_f - h_c = 0$$ (2.8)

This nonlinear algebraic equation can be solved by the Newton-Raphson iterative method (Jain, 2000☰Let Z_2^* be an estimate of Z_2, the Newton-Raphson method gives a better estimate of Z_2 using the following:

$$Z_2' = Z_2^* - \frac{f(Z_2^*)}{f'(Z_2^*)} \qquad (2.9)$$

where:
$$f'(Z_2^*) = 1 - \beta_2 \frac{V_2^2}{gR} - \frac{\partial h_f}{\partial Z_2} \qquad (2.10)$$

After the first 2 iterations, the derivative in Eq (2.10) is computed by using the previous 2 values of $f(Z_2)$. After the updated Z_2' is found, it is checked to see if the flow at that cross section is supercritical. If it is, then the depth is set to either critical depth or normal depth.

The iteration continues until a preset accuracy is obtained. The model automatically switches to a bisection method if the method described above does not reach a convergent solution. The bisection methods guarantees a converged solution.

2.2 Normal Depth Method

With normal depth method, the water depth and velocity can be determined for a given discharge by using the continuity equation and momentum equation:

$$Q = AV \qquad (2.11)$$

$$V = \frac{C_m}{n} R^{2/3} S^{1/2} \qquad (2.12)$$

Where

Q = flow discharge;

V = flow velocity;

A = cross-sectional area assuming a trapezoidal channel with $A = (W_b + H / S_b)H$;

W_b = channel bottom width;

H = flow depth;

S_b = channel bank slope;

n = Manning's coefficient;

C_m = 1.486 for English units or 1.0 for SI units;

R = hydraulic radius (A/P);

P = wetted perimeter ($W_b + 2\sqrt{H(1 + 1/S_b)}$; and

S = channel slope.

3. Bank Erosion Solution

This chapter describes methods to compute the bank erosion rate in SRH-Meander. SRH-Meander provides two types of bank erosion solutions, unit stream power minimization method of Randle (2004) and Linearization Analyses of Johannesson and Parker (1989).

3.1 Unit Stream Power Minimization Method of Randle (2004)

3.1.1 Calculation of Bank Erosion Rate

Randle (2004) proposed a bank erosion model by linking the bank erosion rate with the sediment concentration and by linking the secondary flow phase lag with the minimum unit stream power. In this model, the bank erosion is a function of the channel hydraulic properties to erode the bank and the bank material properties to resist the erosion. The erosion rate is assumed to be linearly related to the flow velocity. The driving force for bank erosion is assumed to be related to the product of the sediment transport capacity and the local curvature. The resisting forces are assumed to be the riparian vegetation, large woody debris, cohesive soils, and bank armoring. It should be cautioned that this method has not been verified with laboratory or field data. The equation used to predict the bank erosion at a distance $s_0 + \Delta s$ along the river is given as:

$$E_b(s_0 + \Delta s) = \left\{ \left[a_1 C_s \left(\frac{W_b}{R_c} \right) \right]_{s=s_0} - \left[\begin{array}{c} a_2 \left(r_\gamma \frac{r_d}{h_b} \right) + a_3 \left(LWD \frac{d_W}{D} \right) \\ + a_4 (PI) + a_5 \left(d_c \frac{h_b}{D} \right) \end{array} \right]_{s=s_0+\Delta s} \right\} a_6 V(s_0) \qquad (3.1)$$

where:

E_b = rate of bank erosion [L/T];

C_s = bed-material sediment concentration [ppm];

W_b = bankfull channel width [L];

R_c = channel radius of curvature [L];

s = distance along the channel;

Δs = planform phase lag distance along the channel;

r_γ = percentage of bank area covered by vegetation roots [%];

r_d = vegetation root depth [L];

h_b = bank height [L];

LWD = percentage of bank area covered by trees or large woody debris [%];

d_W = average height of large woody debris jams [L];

D = hydraulic depth of the channel [L];

PI = plasticity index;

d_c = percentage of bank sediment too coarse for incipient motion [%];

V = mean channel velocity [L/T]; and

$a_1, a_2, a_3, a_4, a_5,$ and a_6 = empirical weighting coefficients.

A unique feature of this model is the computation of the phase lag. The phase lag distance, Δs, is the distance downstream of s where the bank erosion rate is applied. Basically, the driving forces of bank erosion (the velocity and sediment concentration) are computed at s and then the bank resistive forces are computed at $s + \Delta s$ where the bank erosion rate is applied. The phase lag is computed assuming that the river will tend towards the slope that gives the minimum unit stream power:

$$\Delta s = \frac{S_v - S_c}{S_v - S_{minVS}} C_{PL}\left(\frac{\Omega\lambda}{4}\right) \qquad (3.2)$$

where S_v = valley slope;

S_c = channel slope;

S_{minVS} = channel slope at minimum unit stream power, VS;

λ = meander wavelength ($\lambda/4$ is half the distance between river crossings);

Ω = channel sinuosity; and

C_{PL} = a phase-lag coefficient, normally equal to 1.0.

3.1.2 Calculation of Minimum Unit Stream Power

Yang and Song (1979) introduced the unit stream power minimization method based on the energy dissipation theory. The energy dissipation theory states that for a closed and dissipative system in dynamic equilibrium, its energy dissipation rate must be at its minimum value. Yang and Song (1979) proved that for open

channel hydraulics, the minimum energy dissipation rate theory can be simplified to the minimum unit stream power theory if the velocity V and slope S are fairly uniform. The minimum unit stream power theory states that given enough time, an alluvial river will adjust its velocity, slope, roughness, and geometry to reach an equilibrium state such that only minimum unit stream power is used to transport given flow and sediment discharges.

In steady uniform open channel flow, the water depth and velocity can be determined for a given discharge by using the continuity equation and momentum equation given in Eq. 2.11 and 2.12.

The sediment discharge can be calculated by a sediment transport equation. A sediment transport equation is usually based on the velocity, shear stress, or the unit stream power. Here, Yang's (1973 and 1984) sediment transport equations for sand and gravel based on unit stream power are used as an example,

$$\text{Log} C_s = I + J\text{Log}\left[\frac{VS}{\omega} - \frac{V_{cr}S}{\omega}\right] \qquad (3.3)$$

where,

C_s = the sediment concentration of the bed-material load, in ppm;

V_{cr} = the critical mean velocity required for sediment incipient motion;

ω = the fall velocity of the sediment particles; and

I, J = coefficients based on the shear velocity and sediment fall velocity.

Basically we have 3 equations with 4 unknowns, V, H, W_b, and S. The independent variables are Q, C_s (= Qs/Q), and ω. This equations can be solved when the minimum unit stream power theory is applied, i.e.

$$VS = \text{a minimum} \qquad (3.4)$$

A bisection method is used to solve these four equations, and the solution procedure is given here (Figure 3.1).

START

Given minimum and maximum channel bottom width W_b

Given minimum and maximum channel depth H

Calculate V and S by continuity and momentum equations

Calculate sediment discharge $Q_{s\,cal}$ by sediment transport equation

$abs(Q_{s\,cal}-Q_s) <$ tolerance

N

$Q_{s\,cal} < Q_s, \quad H=(H+H_{min})/2$
$Q_{s\,cal} > Q_s, \quad H=(H+H_{max})/2$

Y

Divide W_b min and W_b max into 7 sections and find W_b with minimum VS

Set $W_{b,\,max} = W_b + \Delta W$ and $W_{b,\,min} = W_b - \Delta W$

$\Delta W <$ tolerance

N

Y

Set $W_{b,\,max} = W_b + \Delta W$ and $W_{b,\,min} = W_b - \Delta W$

End

Figure 3.1. Solution procedure of unit stream power minimization

3.1.3 General Procedure for Unit Stream Power Minimization Method of Randle (2004)

The general procedure for solution of the entire system of equations could be accomplished as follows:
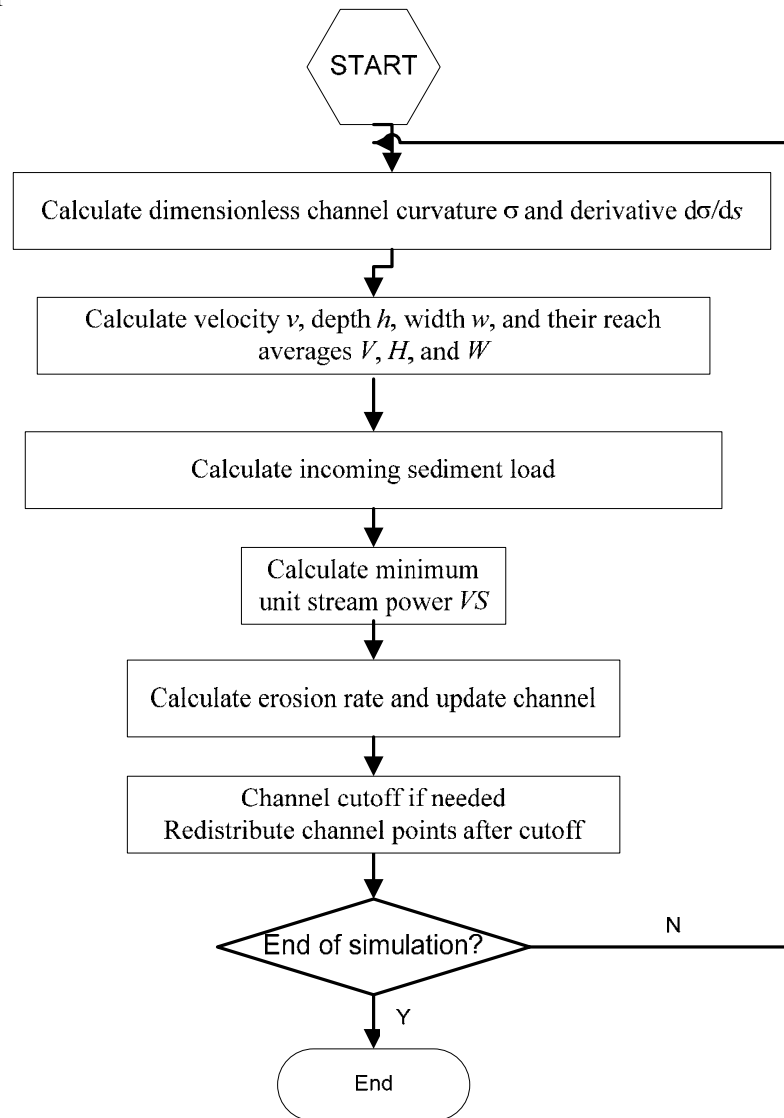
Figure 3.2. Solution procedure of Randle's erosion rate solution based on unit stream power minimization.

3.2 Linearization Analyses of Johannesson and Parker (1989)

One of the most commonly referenced linearization analyses is that by Johannesson and Parker (1989). It is a re-derivation of the analysis by Engelund

(1974). The basic idea behind these analyses is to write the flow variables as a sum of two parts. The first part is the solution to the case of flow in a straight channel. The second part is equal to the deviation from the straight channel solution for the case of a slightly curved channel. The deviation is assumed to be linearly related to the maximum curvature of the channel. These perturbed flow variables are substituted into the 3D flow equations. The equations are then simplified and grouped into the terms responsible for the straight channel solution and those due to the channel curvature. The equations become ordinary differential equations and can be solve analytically or through relatively simple numerical methods. The sediment transport is assumed to be a function of the local velocity and shear stress.

It should be noted that the papers by Zolezzi and Seminara (2001) and Seminara et al. (2001), use a similar technique to Johannesson and Parker (1989), but their derivation accounts for the dispersive transport of momentum by the secondary flow and is not restricted to small perturbations of bed topography. They classify planform development into sub- and super-resonant. The parameter that determines the classification is the width-depth ratio. The width-depth ratio is smaller than the resonant value for the sub-resonant case, and larger for the super-resonant case. For sub-resonant cases, meanders will migrate downstream with an upstream skewed pattern. For the super-resonant case, the meanders will migrate upstream with a downstream skewed pattern. The analysis of Johannesson and Parker basically applies only to the sub-resonant case because it does not incorporate upstream effects of channel pattern. However, because the meanders on the Rio Grande and other major rivers that we have studied migrate downstream, the analysis of Johannesson and Parker is sufficient and the additional complications introduced by the analysis of Zolezzi and Seminara is not deemed necessary.

The perturbation approach has identified many important parameters that define a river's morphology. The decay length, D, was defined by Edwards and Smith (2002) as:

$$D = H/(2C_f) \qquad\qquad (3.5)$$

where D is the decay length, H = average flow depth, and C_f is the friction coefficient. According to Edwards and Smith: "the decay length sets the basic scale for meandering wavelength as well as the distance between channel

inflection points and meander nodes, where meander rate vanishes." In other words, the meander wave length is linearly related to the decay length. The decay length can also be found implicitly in Parker and Johannesson (1989).

There have been several applications using the analyses of Johannesson and Parker (1989). Johannesson and Parker verified their model with data from Muddy Creek. Larsen (1995) applied this model to the Lower Mississippi River and Pole Creek in Wyoming. Larsen et al. (2002) and Thomas (1998) applied this model to the Sacramento River. These implementations have assumed that the flow remains constant. Therefore, it was necessary to determine the effective discharge for channel formation.

The perturbation approach does not assume a wavelength but calculates one based upon the solution of the linearized momentum equations. However, implementations of the perturbation approach general assume that the channel bed slope and hydraulic properties remain constant (Larsen, 1995). This is not strictly required by the theory but usually these implementations assume that the channel does not experience any net aggradation or degradation.

Sun et al. (2001a, b) improved Johannesson and Parker's (1989) linearization theory to calculate bank erosion in river meanders by incorporating multiple-size sediment transport equation. Johannesson and Parker (1989) assume the bank erosion rates are related to the near-bank depth-averaged flow velocity, which is calculated by a small perturbation approach. The near bank depth-averaged flow velocity is decomposed into two parts: the component characterized by local curvature forcing (e.g. point bars) and the component characterized by the free system (e.g. alternate bars).

SRH-Meander adopted the Sun et al. (2001a, b) method which incorporates multiple-size sediment transport equation. However, because the foundation for the analysis is the paper by Johannesson and Parker (1989), the method is referred to as the Johannesson and Parker's method in this manual.

3.2.2 Theory of Linearization Analyses

The velocity field is written as:

$$\widetilde{u} = \overline{u}(\widetilde{s},\widetilde{n})T(\zeta) \tag{3.6}$$

$$\widetilde{v} = \overline{v}(\widetilde{s},\widetilde{n})T(\zeta) + \widetilde{\upsilon}(\widetilde{s},\widetilde{n},\zeta) \tag{3.7}$$

where:

$\tilde{s}$ = streamwise distance;

$\tilde{n}$ = transverse distance;

ζ = $\tilde{z}/\tilde{h}$;

$\tilde{h}$ = depth;

$\tilde{z}$ = distance upward from bed;

$\tilde{u}$ = streamwise velocity (in s, n, ζ directions);

$\tilde{v}$ = transverse velocity (in s, n, ζ directions);

$\bar{u}$ = depth averaged streamwise velocity (in s, n directions);

$\bar{v}$ = depth averaged transverse velocity (in s, n directions); and

$\tilde{\upsilon}$ = transverse velocity due to secondary currents (in s, n, and ζ directions).

The function, $T(\zeta)$, is the velocity shape function as is given in Engelund (1974) as:

$$T(\zeta) = \frac{\chi + \zeta - \frac{1}{2}\zeta^2}{\chi_1} \tag{3.8}$$

where:

χ_1 = $\alpha/\sqrt{C_f}$;

α = 0.077;

χ = $\chi_1 - \frac{1}{3}$;

C_f = friction coefficient = $gn_r^2 / C_m^2 R_h^{\frac{1}{3}}$;

n_r = Manning's coefficient;

R_h = average hydraulic radius;

g = acceleration of gravity; and

C_m = 1.486 for English, 1.0 for SI.

The velocity shape function is a way to parameterize the vertical variation of the velocity with only one parameter, χ_1.

The variables are made non-dimensional by:

$$(u, \hat{v}, \upsilon) = \frac{(\bar{u}, \bar{v}, \tilde{\upsilon})}{U} \tag{3.9}$$

$$(s, n) = \frac{(\tilde{s}, \tilde{n})}{b} \tag{3.10}$$

$$(\xi, \eta, h) = \frac{(\widetilde{\xi}, \widetilde{\eta}, \widetilde{h})}{H} \tag{3.11}$$

where:

U = reach averaged velocity;

b = reach averaged half width of channel, assumed constant;

ξ = dimensionless water surface elevation;

η = dimensionless bed elevation;

h = dimensionless depth; and

H = reach averaged depth.

A perturbation analysis to first order is then performed using the non-dimensionalized streamwise and transverse momentum equations where the small parameter is defined as Ψ_0:

Ψ_0 $= b/r_m =$ dimensionless maximum centerline curvature; and

r_m = minimum centerline radius of curvature.

The analysis assumes that $\Psi_0 \ll 1$, which is an assumption inherent in perturbation analyses. If Ψ_0 is not $\ll 1$, then the assumption that the flow variables can be written as linear functions of Ψ_0 is no longer valid. The dimensionless variables are written as the following first order expansions about Ψ_0:

$$(u, v, \upsilon) = (1,0,0) + \Psi_0(u_1, v_1, \upsilon_1) \tag{3.12}$$

$$(h, \xi, \eta) = (1, \xi_r - I_* s, \eta_r - I_* s) + \Psi_0(h_1, \xi_1, \eta_1) \tag{3.13}$$

where:

$I*$ $= I\, b/H,$

I = water surface slope, and

ξ_r, η_r = reference water surface and bed elevations for which $H = \widetilde{\xi}_r - \widetilde{\eta}_r$.

The above expressions were substituted into the three dimensional governing equations, simplified, and grouped according to Ψ_0. The equations governing the water surface elevation and secondary current information were found to be:

$$\xi_1 = -F^2 \chi_{20} n\sigma \tag{3.14}$$

$$\frac{1}{r}\frac{d\sigma_s}{d\phi} + \delta\sigma_s = \delta\sigma \tag{3.15}$$

$$\upsilon_1 = \frac{G_0(\zeta)\sigma_s}{\varepsilon\chi_1} \qquad (3.16)$$

where:

χ_{20} $= \left(\chi^3 + \chi^2 + \frac{2}{5}\chi + \frac{2}{35}\right)\Big/\chi_1{}^3$, $1.01 < \chi_{20} < 1.11$ for $0.01 > C_f > 0.0011$;

F $= U/\sqrt{gH}$, reach averaged Froude number;

σ $= C/\Psi_0$, dimensionless channel curvature;

C $=$ dimensionless channel curvature $= b\widetilde{C}$;

$\widetilde{C}$ $=$ centerline curvature, inverse of radius of curvature, $(d\theta/ds)$;

θ $=$ angle between channel centerline and x-axis;

σ_s $=$ dimensionless secondary current cell strength;

ϕ $=$ phase $= ks;$

s $=$ dimensionless streamwise coordinate;

r $= k/\varepsilon$, reduced wave number;

k $= b2\pi/\widetilde{\lambda}$, dimensionless wave number;

ε $= C_f b/H$;

$\widetilde{\lambda}$ $=$ wave length; and

δ $= \dfrac{\chi_1{}^2\left(\chi + \frac{1}{4}\right)}{\frac{1}{12}\chi^2 + \frac{11}{360}\chi + \frac{1}{504}} \sim O(10)$.

The function $G_0(\zeta)$ is:

$$G_0(\zeta) = \frac{1}{\chi_1{}^2}\left[\begin{array}{c}\left(\chi^2 + \frac{2}{3}\chi + \frac{2}{15}\right)\cdot(\chi + \zeta) - \frac{1}{2}\chi^2\zeta^2 \\ -\frac{1}{3}\chi\zeta^3 - \frac{1}{12}(1-\chi)\zeta^4 + \frac{1}{20}\zeta^5 - \frac{1}{120}\zeta^6\end{array}\right] - \chi_{20}\left[\chi + \zeta - \frac{1}{2}\zeta^2\right] \quad (3.17)$$

According to Johannesson and Parker, the phase shift between the secondary current strength and the channel curvature predicted by Eq.3.15 is typically on the order of 10 degrees. Therefore, it is expected that σ_s does not vary substantially from the local normalized curvature, σ.

To solve for the remaining variables, they developed a C-Problem and an F-Problem corresponding respectively to systems characterized by the local curvature forcing (e.g. point bars) and that characterized by the response of the free system (e.g. alternative bars) to this forcing. The solution for the perturbation values are decomposed into the solution of the C- and F-problems:

$$(u_1, v_1) = (u_{1C}, v_{1C}) + (u_{1F}, v_{1F}) \qquad (3.18)$$

$$(h_1, \eta_1) = (h_{1C}, \eta_{1C}) + (h_{1F}, \eta_{1F}) \qquad (3.19)$$

The ordinary differential equations describing the C-problem are written as

$$\frac{du_{1C}}{d\phi} + 2\varepsilon u_{1C} = -\chi_{20}\frac{d\sigma}{d\phi} - (\varepsilon - \varepsilon\chi_{20}F^2)\sigma + \varepsilon(A + A_s)\sigma_s \tag{3.20}$$

$$\eta_{1C} = -An\sigma_s \tag{3.21}$$

The ordinary differential equations describing the F-problem are written as

$$\frac{d^2 u_{1F}}{d\phi^2} + \left[G_2\left(\frac{\pi}{2}\right)^2 - \varepsilon(G_1 - 3)\right]\frac{du_{1F}}{d\phi} + 2\varepsilon G_2\left(\frac{\pi}{2}\right)^2 u_{1F}$$

$$= -\varepsilon F^2\chi_{20}\frac{d\sigma}{d\phi} - \varepsilon A\frac{d\sigma_s}{d\phi} + \varepsilon(G_1 - 1)\frac{du_{1C}}{d\phi} \tag{3.22}$$

$$\eta_{1Fb} = -r\frac{\partial u_{1Fb}}{\partial\phi} - 2u_{1Fb} \tag{3.23}$$

where:

$$G_1 \quad = \sum_{\Phi} P_{\Phi 0}\frac{3 + 6f(\Phi)}{1 - f(\Phi)};$$

$$G_2 \quad = \frac{1 + \alpha_*\mu}{\mu}\frac{H}{b}\sum_{\Phi} P_{\Phi 0}\sqrt{f(\Phi)};$$

α_* = the ratio of lift coefficient to drag coefficient for a spherical sand particle placed on a rough bed ($\alpha_* \approx 0.85$);

μ = dynamic angle of Coulomb friction ($\mu \approx 0.43$);

$P_{\Phi 0}$ = reach-averaged volume fraction in the surface layer;

$$f(\Phi) \quad = \frac{E(\Phi)\tau^*_{cm}}{C_f T(0)^2};$$

Φ = sediment size defined as $\log_2\dfrac{D_s}{D_{m0}}$;

D_s = grain diameter;

D_{m0} = reach-averaged grain diameter;

$$E(\phi) \quad = \begin{cases} 2^\Phi/(1 + 0.2354\phi)^2 & \phi > -1.32 \\ 0.843 & \phi < -1.32 \end{cases};$$

$$\phi \quad = \frac{\tau^*_m}{\tau^*_{cm}} = \frac{\tilde{\tau}_s}{\tilde{\tau}_{cm}} = \frac{\rho C_f\sqrt{\tilde{u}_{bs}^2 + \tilde{u}_{bn}^2}\,\tilde{u}_{bs}}{\tilde{\tau}_{cm}};$$

τ^*_{cm} = critical Shields shear stress for transport of sediment with a mean grain size of D_{m0}; and

$$T(\zeta) \quad = \frac{\chi + \xi - \frac{1}{2}\xi^2}{\chi_1}.$$

3.2.3 Numerical Methods for Linearization Analyses

Dimensionless secondary current cell Strength σ_s is calculated by the analytical solution as,

$$\sigma_s = \sigma_s(0)\exp(\varepsilon\delta s) + \int_0^s \varepsilon\delta\sigma(s_1)\exp[\varepsilon\delta(s - s_1)]ds_1 \qquad (3.24)$$

The integration can be calculated by the trapezoidal method as

$$\sigma_s(i) = \sigma_s(0)\exp(\varepsilon\delta s) + \varepsilon\delta\sum_{j=2}^{i} \sigma_{j-1/2}\exp(\varepsilon\delta\Delta s_j)\Delta s_j \qquad (3.25)$$

where:

$\sigma_{j-1/2}$ = average value of σ between cross sections j-1 and j; and

Δs_j = dimensionless distance between cross sections j-1 and j.

C-velocity

The ordinary differential equation for the C-problem Eq.3.20 is solved by the Fourth-Order Runge-Kutta Method, written as

$$u_{1C\,i+1} = u_{1C\,i} + \left[\frac{1}{6}(k_1 + 2k_2 + 2k_3 + k_4)\right]\Delta s \qquad (3.26)$$

where:

$k_1 \quad = -2\varepsilon u_{1C\,i} + \text{RHS}\,;$

$u_{1C1} \quad = u_{1C\,i} + \frac{1}{2}k_1\Delta s\,;$

$k_2 \quad = -2\varepsilon u_{1C1} + \text{RHS}\,;$

$u_{1C2} \quad = u_{1C1} + \frac{1}{2}k_2\Delta s\,;$

$k_3 \quad = -2\varepsilon u_{1C2} + \text{RHS}\,;$

$u_{1C3} \quad = u_{1C2} + \frac{1}{2}k_3\Delta s\,;$

$k_4 \quad = -2\varepsilon u_{1C3} + \text{RHS}\,;$ and

RHS = right hand side of Eq.3.20.

Due to large spatial distance between cross sections, the Fourth-Order Runge-Kutta Method is performed in smaller intervals by dividing the distance between cross sections into smaller steps.

F-velocity

The second-order ordinary differential equation for the F-problem, Eq.3.22 can by simplified by a set of first-order ordinary differential written as

$$\frac{du_{1F}}{ds} = Y \tag{3.27}$$

$$\frac{dY}{ds} = -AA \cdot Y - BB \cdot u_{1F} + \text{RHS} \tag{3.28}$$

where:

$$AA = \left[G_2 \left(\frac{\pi}{2} \right)^2 - \varepsilon(G_1 - 3) \right];$$

$$BB = 2\varepsilon G_2 \left(\frac{\pi}{2} \right)^2 ; \text{ and}$$

$$\text{RHS} = \text{right hand side of Eq.3.22.}$$

The fourth-order Runge-Kutta Method can be modified to solve the equation set of one-order ordinary differential equation. The four steps of the method can be summarized as,

Step 1:
$$k_{11} = Y_{i-1} ;$$
$$k_{12} = -AA \cdot Y_{i-1} - BB \cdot u_{1F\ i-1} + \text{RHS} ;$$
$$u_{1F1} = u_{1F\ i-1} + \frac{1}{2} k_{11} \Delta s ; \text{ and}$$
$$Y_1 = Y_{i-1} + \frac{1}{2} k_{12} \Delta s .$$

Step 2:
$$k_{21} = Y_1 ;$$
$$k_{22} = -AA \cdot Y_1 - BB \cdot u_{1F1} + \text{RHS} ;$$
$$u_{1F2} = u_{1F1} + \frac{1}{2} k_{21} \Delta s ; \text{ and}$$
$$Y_2 = Y_1 + \frac{1}{2} k_{22} \Delta s .$$

Step 3:
$$k_{31} = Y_2 ;$$
$$k_{32} = -AA \cdot Y_2 - BB \cdot u_{1F2} + \text{RHS};$$
$$u_{1F3} = u_{1F2} + \frac{1}{2} k_{31} \Delta s ; \text{ and}$$

$$Y_3 = Y_2 + \frac{1}{2} k_{32} \Delta s .$$

Step 4:

$$k_{41} = Y_3 ;$$

$$k_{42} = -AA \cdot Y_3 - BB \cdot u_{1F3} + \text{RHS} ;$$

$$u_{1F\ i} = u_{1F\ i-1} + \left[\frac{1}{6} (k_{11} + 2k_{21} + 2k_{31} + k_{41}) \right] \Delta s ; \text{ and}$$

$$Y_i = Y_{i-1} + \left[\frac{1}{6} (k_{12} + 2k_{22} + 2k_{32} + k_{42}) \right] \Delta s .$$

Due to large spatial distance between cross sections, the Fourth-Order Runge-Kutta Method is performed in smaller intervals by dividing the distance between cross sections into smaller steps.

3.2.4 General procedure for Linearization Analyses

The general procedure for solution of the entire system of equations could be accomplished as follows (Figure 3.3):
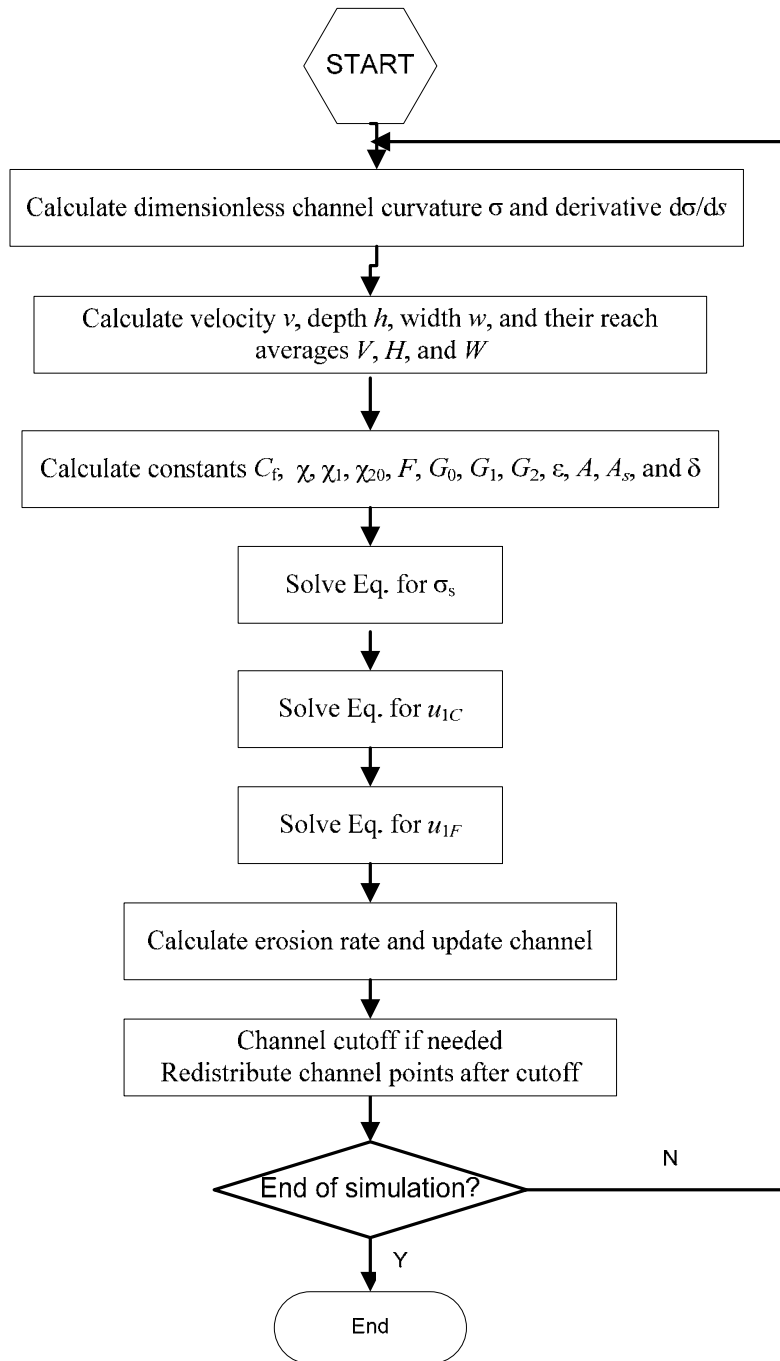
Figure 3.3. Solution procedure for the method of Johannesson and Parker.

4. Channel Migration

This chapter describes the methods used to update the channel position in SRH-Meander. First, the channel bank erosion rate is calculated if the linearization analyses of Johannesson and Parker (1989) is used. Then, the channel is updated, followed by the channel cutoff if it is needed. Finally, points representing the channel alignment are redistributed.

4.1 Erosion Rate

Ikeda et al. (1981) assumed that the bank erosion rate was linearly related to the deviation in velocity from the mean velocity:

$$E_b = E_0 u_b \qquad (4.1)$$

where:

E_b = rate of bank erosion [L/T];

u_b = deviation from mean velocity at bank [L/T]; and

E_0 = bank erosion constant [-].

Hasegawa (1989) derived the following equation based upon an analysis of the sediment continuity equation and using the bed load equation of Meyer-Peter and Muller (1948):

$$E_b = \frac{q_s}{(1-\lambda)h}\left\{ \frac{3h\phi_*}{\tan\phi_k}\left[\underbrace{\frac{\partial u/U}{\partial s}}_{1} - \underbrace{\frac{1}{6}\frac{\partial \eta/h}{\partial s}}_{2} \right] + T\tan\theta_k\left[\underbrace{3\phi_*\frac{u}{U}}_{3} - \underbrace{\frac{\eta}{h}(0.5\phi_*+1)}_{4} - \underbrace{\frac{h_f}{h}}_{5} \right] - \underbrace{\left(\frac{v}{U}+\tan\psi\right)}_{6} \right\}_{n=n_T} \qquad (4.2)$$

where some of the variables are defined in Figure 4.1:

E_b = rate of bank erosion [L/T];

q_s = unit bedload transport rate [L^2/T];

h = average depth;

u = velocity deviation from mean velocity U;

U = cross section average velocity;

v = transverse component of the flow velocity average over depth;

ψ = deviation angle of direction of the near-bottom flow from the *s*-axis due to secondary currents;

η = distance from mean depth to thalweg;

n = transverse distance;

s = streamwise distance;

T = $\sqrt{\tau_{*c}/(\mu_s \mu_k \tau_{*0})}$;

θ_k = angle of transverse slope;

λ = porosity;

ϕ_* = $\dfrac{\tau_{*0}}{\tau_{*0} - \tau_{*c}}$;

τ_{*0} = non-dimensional shear stress;

τ_{*c} = critical non-dimensional shear stress;

μ_s = coefficient of static friction; and
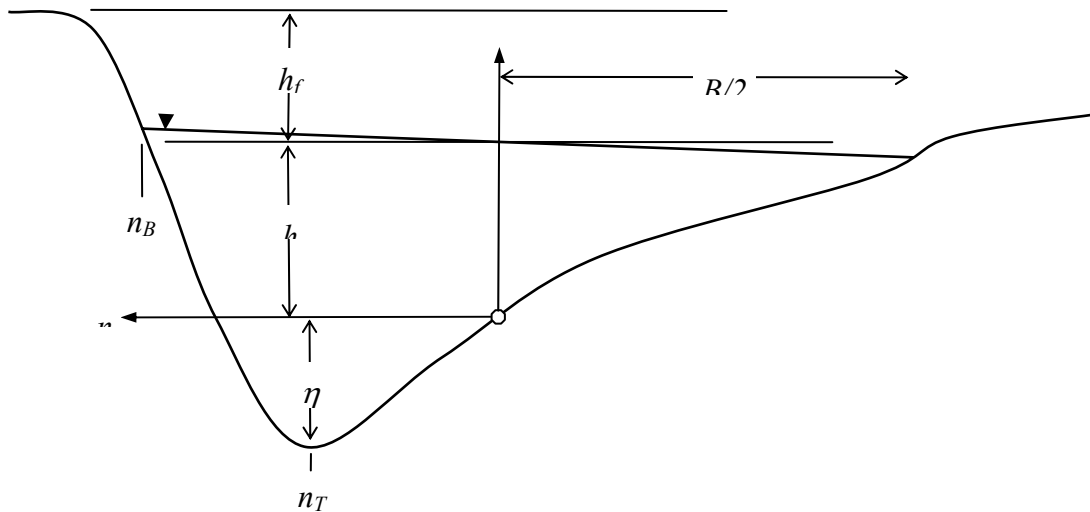
μ_k = coefficient of dynamic friction.

Figure 4.1. Definition of variables in Hasegawa bank erosion relationship.

The terms were explained by Hasegawa as (1) longitudinal rate of change of flow velocity, (2) longitudinal rate of change of bed elevation, (3) the relative magnitude of the perturbed component of flow velocity near the bank, (4) the relative depth of bed scour, (5) relative bank height, and (6) the relative magnitude of the transverse component of near-bottom flow velocity. He goes on to ignore all the terms in the equation except for (3), and substitute the Meyer-Peter-Muller formula in for q_s, which gives:

$$E_b = u_b \sqrt{C_f} I_0 \left[\frac{3KT \tan \theta_k}{(1-\lambda)(\rho_s/\rho - 1)\sqrt{\phi_*}} \right] \tag{4.3}$$

where:

  K = coefficient in bed load equation;
  C_f = friction coefficient; and
  I_0 = average bed slope.

Hasegawa further simplifies (4.3) by grouping the bracketed terms into a single parameter, E_*, which is assumed to encompass the bank strength and erosive properties:

$$E_b = \sqrt{C_f} I_0 E_* u_b \tag{4.4}$$

However, if the bank height is large and varies throughout the reach, it may be beneficial to include terms (4) and (5) into the bank erosion equation as follows:

$$E_b = \frac{q_s}{(1-\lambda)h} T \tan \theta_k \left[3\phi_* \frac{u}{U} - \frac{\eta}{h}(0.5\phi_* + 1) - \frac{h_f}{h} \right] \tag{4.5}$$

where high banks and deep scour holes tend to suppress bank erosion.

Howard (1995) implemented the meander model of Johannesson and Parker (1989) and used the following for the erosion rate:

$$E_b = K_r K_l \varphi (V u_b + D h_t) Q_f [1 - B \cos(A)] / R_b \tag{4.6}$$

where:

  K_r = nominal erosion rate [-];
  K_l = local bank erodibility [-];
  φ = total sinuosity correction [-];
  V = velocity weight [-];
  u_b = total near bank velocity perturbation [L/T];
  D = depth weight [-];

h_t = relative depth [-];

Q_f = discharge correction factor [-];

B = directional bias factor (usually 0);

A = angle of local flow [-]; and

R_b = bank erosion resistance [-].

The erosion rate of Howard (1995) allows bank erosion even when $u_b = 0$, if $D > 0$. Therefore, bank erosion can occur in a straight channel as well. Howard's model essentially includes terms 3 and 5 from the Hasegawa model of bank erosion (Eq. 2.3). Howard (1995) also incorporated chute cutoffs, channel aggradation and changes to the channel slope. There are many more calibration parameters in the model of Howard than Ikeda et al. (1981).

Lancaster (1998) assumes that the bank erosion rate is proportional to the deviation of the bank shear stress from the mean shear stress:

$$E_b = E_0 \bar{\tau}_b \cdot \hat{n}_t \tag{4.7}$$

where:

E_b = rate of bank erosion [L/T];

E_0 = bank erosion constant [L^{2}T/M];

$\bar{\tau}_b$ = shear stress deviation from mean velocity at bank [M/L/T^2]; and

$\hat{n}_t$ = unit vector along bank line [-].

The shear stress is usually assumed to be related to the square of the velocity ($\bar{\tau}_b = \frac{1}{2}\rho C_f |\bar{u}_b| \bar{u}_b$).

All the meander models described above assume the river maintains a constant width. Therefore, the erosion of the outer bank is balanced by deposition along the inner bank. Also, there is a general assumption that the bank erosion is not affected by upstream sediment supply. In the case of the Rio Grande, this may cause problems because the river may be increasing its sinuosity and decreasing its slope in response to a decrease in sediment supply. The perturbation approaches as stated above do not even require sediment supply as part of their input.

SRH-Meander uses the erosion rate given by Ikeda et al. (1981) when linearization analyses method of Johannesson and Parker (1989) is used. Other erosion rate methods are reviewed here and can be incorporated into SRH-Meander in the future.

Randle's method calculates the erosion rate directly considering the driving force and resisting forces to the bank erosion.

4.2 Channel Update

Each point defining the channel centerline is moved perpendicular to the local tangent of the channel centerline. The bank erosion rate defines the distance the point moves. SRH-Meander adopts the geometrical method of Camporeale et al. (2005). The updated channel can be expressed as,

$$x_i(t + \Delta t) = x_i(t) - \zeta \frac{b}{c} \tag{4.8}$$

$$y_i(t + \Delta t) = y_i(t) + \zeta \frac{a}{c} \tag{4.9}$$

where:

x_i, y_i = coordinate of the ith point;

t = time;

Δt = time step;

ζ = normal displacement ($= E u_b \Delta t$);

a = $x_{i+1}(t) - x_{i-1}(t)$;

b = $y_{i+1}(t) - y_{i-1}(t)$; and

c = $\sqrt{a^2 + b^2}$.

4.3 Channel Cutoffs

A channel cutoff occurs when a river abandons an existing portion of its length to find a new shorter path. Accurate modeling of a channel cutoff usually requires information on bank protection, floodplain topography, and riparian vegetation. The exact location of a channel cutoff is inherently difficult to predict because of the large number of variables that control it.

To simplify the simulation of cutoffs, SRH-Meander provides only two kinds of cutoffs: auto and manual. An auto cutoff is performed when the ratio of the length of channel to the length of the valley exceeds a threshold value input by the user. A manual cutoff will occur at a user specified time and location to link two points in the channel.

A straight line is used to link the two points of the channel during the cutoff.

After the cutoff, points are redistributed along the channel at equal distances.

4.2 Channel Points Redistribution

The channel alignment line is redistributed according to cubic spline interpolation (Press et al, 1992). Since the same x-coordinate of the channel alignment line may have multiple values of y-coordinates, the interpolation is performed for x and y coordinates with respect to the channel length s. The equations given in the following for the y-coordinate can also be used for the x-coordinate. Cubic spline interpolation shows that the dependence of y on the independent variable s is through the linear s-dependence of A and B, and the cubic s-dependence of C and D. Cubic spline interpolation gives the interpolation formula in an interval as

$$y = Ay_i + By_{i+1} + C\frac{d^2 y_i}{ds^2} + D\frac{d^2 y_{i+1}}{ds^2} \qquad (4.10)$$

where:

$$A = \frac{s_{i+1} - s}{s_{i+1} - s_i};$$

$$B = 1 - A = \frac{s - s_i}{s_{i+1} - s_i};$$

$$C = \frac{1}{6}(A^3 - A)(s_{i+1} - s_i)^2;$$

$$D = \frac{1}{6}(B^3 - B)(s_{i+1} - s_i)^2; \text{ and}$$

$$s = \text{channel streamwise coordinate.}$$

To calculate the value of y between points i and $i+1$, one needs to know the second derivative, $\dfrac{d^2 y}{ds^2}$, of the new interpolating polynomial.

The first derivative is obtained by taking derivatives of Eq. 4.10 with respect to s,

$$\frac{dy}{ds} = \frac{y_{i+1} - y_i}{y_{i+1} - y_i} - \frac{3A^2 - 1}{6}(s_{i+1} - s_i)\frac{d^2 y_i}{ds^2} + \frac{3B^2 - 1}{6}(s_{i+1} - s_i)\frac{d^2 y_{i+1}}{ds^2} \qquad (4.11)$$

The second derivative is obtained by setting Eq. 4.11 evaluated for $s = s_i$ in the interval (s_{i-1}, s_i) equal to the same equation evaluated for $s = s_i$ in the interval (s_i, s_{i+1}). This gives the equation for $\dfrac{d^2 y}{ds^2}$ at $I = 2, \ldots, N\text{-}1$

$$\frac{s_i - s_{i-1}}{6}\frac{d^2 y_{i-1}}{ds^2} + \frac{s_{i+1} - s_{i-1}}{3}\frac{d^2 y_i}{ds^2} + \frac{s_{i+1} - s_i}{6}\frac{d^2 y_{i+1}}{ds^2} = \frac{y_{i+1} - y_i}{s_{i+1} - s_i} - \frac{y_i - y_{i-1}}{s_i - s_{i-1}} \qquad (4.12)$$

There are N-2 linear equations in the N unknowns of $\dfrac{d^2 y_i}{ds^2}$, $I = 1,\ldots, N$. SRH-Meander assumes that boundary conditions at s_1 and s_N as $\dfrac{d^2 y_1}{ds^2} = 0$ and $\dfrac{d^2 y_N}{ds^2} = 0$.

SRH-Meander redistributes the channel curve to equally spaced points after every time step.

5. Terrain Elevation Change

SRH-Meander can also calculate the terrain elevation changes after the channel migration. The sediment mass balance is enforced using the incoming sediment, outgoing sediment, bank erosion and deposition, and bed erosion or deposition. This also involves information exchanges between 1D meandering river data and 2D terrain data.

5.1 Sediment Mass Balance

Sediment mass balance is considered between two cross sections. If the cross sections are far apart relatively it can be acceptable to assume that the bed-material load discharge equals to the sediment transport capacity of the flow; i.e., the bed-material load is transported in an equilibrium mode ($Q_s = Q^*$, where Q^* is the transport capacity). In other words, the exchange of sediment between the bed and the fractions in transport is instantaneous. However, the spatial-delay and/or time-delay effects are important in circumstances where there are rapid hydraulic changes in short reaches. To model these effects, SRH-Meander uses the analytical solution of Han (1980) to calculate the sediment concentration:

$$C_i = C_i^* + (C_{i-1} - C_i^*)\exp\left\{-\frac{V_d W_i \Delta x}{Q_i}\right\}$$
(5.1)

where C = computed discharge weighted average sediment concentration; C_i^* = the computed sediment transport capacity concentration; Q_i = flow rate; V_d = deposition velocity; W_i = channel top width; Δx = reach length; and i = cross-section index (increasing from upstream to downstream). Eq. (5.1) is employed for each of the particle size fractions. The volume of sediment deposition, ΔV_s, in a reach is calculated from (for erosion ΔV_s would be negative):

$$\Delta V_s = (Q_{si-1} - Q_{si})\Delta t = (Q_{i-1}C_{si-1} - Q_i C_{si})\Delta t$$
(5.2)

The volume of deposition is geometrically approximated by:

$$\Delta V_s = A^n \Delta z_b - h_l s_l \Delta n_l + h_r s_r \Delta n_r$$
(5.3)

where:

Δz_b = bed elevation change;

A = plan area of river bed;

n_l, n_r = lateral location of left and right banks;

s_l, s_r = length of left and right banks; and

h_l, h_r = height of left and right banks, during deposition it is the bank height under water.

SRH-Meander assumes that the channel cross sectional geometry is unchanged during the channel migration. If bank erosion occurs on one side of channel, there is deposition up to the water surface elevation on the other side, and the channel width is unchanged.

Sediment mass balance is enforced by equalizing the sediment deposition calculated from Eqs. (5.2) and (5.3), and the bed elevation change Δz_b is computed with the following equation.

$$A^n \Delta z_b - h_l s_l \Delta n_l + h_r s_r \Delta n_r = \left(Q_{i-1}C_{si-1} - Q_i C_{si}\right)\Delta t \qquad (5.4)$$

5.2 Interaction between Meandering River and Terrain

The terrain elevation and sediment fraction are represented by a square grid generated using ARC-GIS raster file. The interaction between the meandering river and terrain involves the information exchange between left and right banks and terrain. The method to identify their relationships follows Sun et al. (2001b):
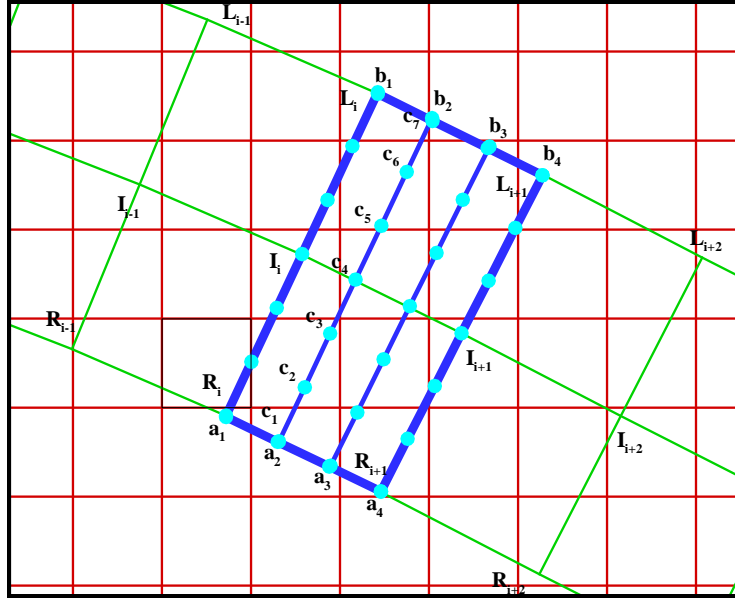
Figure 5.1. Interaction between river and terrain

1. The central line is represented by a sequence of points $\{I_i\}$, i=1, 2, … N. The central line is shaft to left a distance of $\{W_i/2\}$, i=1, 2, … N, where W_i is the channel top width of cross section i, using the same equations as Eqs. (4.8) and (4.9), to find the left bank points. The left bank points is represented by a sequence of points $\{L_i\}$, i=1, 2, … N. The same procedure is used to find right bank points $\{R_i\}$, i=1, 2, … N.

2. The length of the left bank segment i (between cross sections i and i+1) is compared with the length of the right bank of the same segment to find the longest of the two $L_{\max}$. The two bank segments are divided into J $(=L_{\max}/a+1)$ points, where a is the grid size used. The interpolated points are named a_1, a_2, …, a_J in right bank and b_1, b_2, …, b_J in the left bank. If points a_j is located in cell $C_{i,j}$, cell $C_{i,j}$ is associated with left bank of river segment i. The cells and the number of cells associated with left bank segment i and right bank segment i are each stored in an array.

3. Line a_jb_j is divided into K $(=a_jb_j/a+1)$ points, represented by c_1, c_2, …, c_K. If points c_k is located in cell $C_{i,j}$, cell $C_{i,j}$ is associated with cross section i. The cells and the number of cells associated with river segment i (between cross sections i and i+1) are stored in an array.
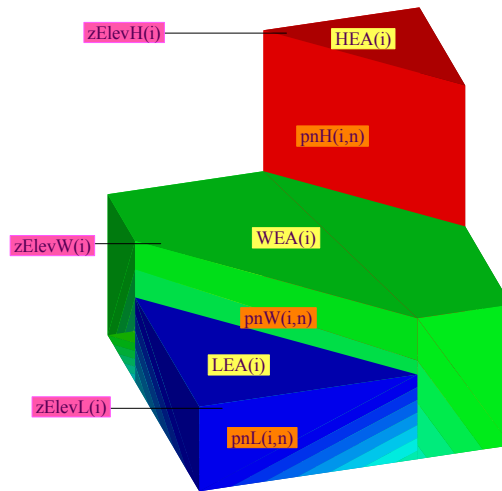
5.3 Terrain Information

Figure 5.2. Scheme to represent a grid cell

Figure 5.2 shows the scheme used to represent a terrain grid cell. During the bank migration, the bank line sweeps only a small fraction of a grid cell. A uniform cell elevation and sediment size fraction does not characterize this circumstance. SRH-M divides a cell element into three separate areas: low elevation area (LEA), water surface elevation area (WEA), and high elevation area (HEA). LEA represents the area of river bed. WEA represents the area that is newly deposited sediment up to the water surface elevation. HEA represents the original elevation area of the eroding bank. The elevation, area percentage, and sediment size distributions of the three types of area in a cell is stored in memory. The final cell properties are weighted average of these three areas.

After each step of channel migration, the area migrated by each bank segment from cross section i to cross section $i+1$ is calculated as the product of the bank length and the lateral migration distance. This area is then redistributed along all the cells that the bank segment located to be the erosion or deposition area in a cell, named cell erosion area (CEA) or cell deposition area (CDA).

To calculate the bank erosion volume in a grid cell, firstly the CEA is eroded from WEA. Secondly, if CEA is larger than WEA, the remaining area is eroded from HEA. Finally, if CEA is larger than WEA+HEA, the remaining area is redistributed along the other cells associated with the bank segment. The eroded volume is calculated considering the bank migration will erode the terrain to the bed elevation at this river cross section. Terrain elevation and sediment size

distribution are also updated during the bank erosion.

To calculate the bank deposition volume in a grid cell, the CDA is deposited into LEA. If CDA is larger than LEA, the remaining area is redistributed along the other cells located by the bank. The deposition volume is calculated considering the bank migration deposits sediment to the water surface elevation at this river cross section. Terrain elevation and sediment size distribution are also updated during the bank deposition.

The cell elevation associated with river cross section i is updated with Eq. (5.4). In the same way with bank cells, erosion occurs in WEA and HEA and deposition occurs in only LEA. Eq. (5.4) is used for each sediment size fractions and an active layer concept is used to update the sediment size distributions at the bed.

The active layer is defined as a thin upper zone of constant thickness that is user predefined. The thickness of the active layer can control the rate at which the bed armors.

6. Running SRH-Meander

6.1 Input Data Format

SRH-Meander reads a main ASCII input file and several ARC-GIS files. The main input file is organized in sequential records. The sequence is presented in a flow chart in Appendix A. A record is a line of up to 300 characters in length. A line starting with "***" is a comment line and will be ignored by the model. A record starts with a specific record name containing 3 characters. Each record name is unique and inputs specific data to the program. A comprehensive list of all records names used by SRH-Meander is given in Appendix B. A detailed explanation of all the records is given in Appendix C. Not all records are used (for example, some are mutually exclusive) but they have to be in an appropriate sequence.

Data after the record name is in an unformatted form to prevent unnecessary errors. Error checking is provided to prevent some human errors, which include:
- empty lines;
- lines started with space instead of the record name;
- incorrect record names;
- incorrect number of data following the record name; and
- incorrect data values.

The data are prepared in ASCII files. For easy data input, examples are provided in Microsoft EXCEL format. Users may save the data in type of "Text Formatted (Space delimited) *.prn". It is recommended that the user study the example input files included in the distribution of SRH-Meander to become familiar with the input data format. The EXCEL sample input files also contain the explanation of each variable in the comment field.

Other input files include:

1. Arc GIS point shapefile for initial channel central line with selected options that "Coordinates will contain M value" and "Coordinates will contain Z value". User may refer to Appendix H to learn how to generate these files. An ArcGIS shapefile contains several files and only file with extension *shp* is required.

2. Arc GIS point shapefile for final channel central line with selected options

that "Coordinates will contain M value" and "Coordinates will contain Z value". User may refer to Appendix H to learn how to generate these files. An ArcGIS shapefile contains several files and only file with extension *shp* is required. This file is Optional.

3. Arc GIS point shapefile for valley axis with selected options that "Coordinates will contain M value" and "Coordinates will contain Z value". User may refer to Appendix H to learn how to generate these files. An ArcGIS shapefile contains several files and only file with extension *shp* is required.

4. ArcGIS shapefile for meandering environmental parameter with selected options that "Coordinates will contain M value" and "Coordinates will contain Z value". Two files with the same name but different extensions as ****.shp*, and ****.csv* are required. ****.shp* contains the polygon geometry information. ****.csv* contains the field values associated with related polygons. User may refer to MEN record descriptions to learn the field names of this polygon file. User may also refer to Appendix I to learn how to generate this ArcGIS polygon shapefile.

5. ASCII ArcGIS raster file for terrain elevation. This file is optional required only when the terrain elevation change is calculated. User may also refer to Appendix J to learn how to generate this ASCII ArcGIS raster file.

6.2 Executing SRH-Meander

After preparing the input data file, SRH-Meander can be executed within windows by double-clicking the filename in Windows Explorer. SRH-Meander can also be used from the command line interface. At the prompt, simply type:

C:\> SRH-Meander.EXE FILENAME.DAT

or

C:\> SRH-Meander.EXE –e FILENAME.DAT

The argument "-e" in the commend line forces the program to exit all windows when the program is terminated.

Make sure the executable exist in the system PATH variable. If SRH-Meander is launched without an input file name, the program prompts the user to enter it. For consistency, the input data file should have an extension .DAT (or .dat), but the program will work with any other extension. The FILENAME.DAT argument can

also include the drive letter and path information if the entire string is encapsulated by quotes.

SRH-Meander displays the current bed profile and channel profile during the simulation. Using this real time display, one can monitor the simulation during a run. This feature is useful in debugging and calibrating.

6.3 Output Files

For a given input file named sample.dat, the following files may be generated.

sample_OUT.dat: the *_OUT.dat file echoes the input data. When an error occurs on reading the input files, the users should first check this file for possible warnings.

sample_Raster.dat: the *_Raster.dat file is the terrain raster file, which contains the x, y, and z coordinate of the terrain. This file is empty if there is no terrain calculation.

sample_Centerline.dat: the *_Centerline.dat file contains the cross section number, cross section location x and y, thalweg elevation, left bank height, right bank height, channel slope, water depth, section length, left bank length, right bank length, curvature, left bank curvature, right bank curvature, phase lag, and erosion coefficient.

sample_ErosionData.dat: the *_ErosionData.dat file contains the cross section number, cross section location x and y, thalweg elevation, water surface elevation, active layer thickness, cross sectional averaged depth, thalweg depth, left bank height, right bank height, velocity deviation, erosion coefficient, and concentration.

sample_ErosionVolume.dat: the *_ErosionVolume.dat file contains the time, bank erosion volume, and area that channel has migrated. This file is empty if there is no terrain calculation.

sample_Envelop.dat: the *_Envelop.dat file is the envelop file, which contains the initial channel with left and right banks, final channel with left and right banks, the envelop channel which represents the migration area the left and right banks migrated in the whole simulation. This file is empty if there is no terrain calculation.

7. Examples

Three examples are presented here: the first one on a laboratory channel migration, the second on the Middle Rio Grande, and third one on the Sacramento River.

7.1 Laboratory Channel Migration

SRH-Meander is used to simulate the channel migration in a controlled laboratory study (U.S. Army Corps of Engineers, 1945). The study itself consisted of a myriad of tests attempting to isolate and adjust individual variables to better understand channel migration response. The following discussion refers to one test in particular, titled 'Effect of Not Feeding Sand at the Entrance'. This test was chosen to be used for calibration because of the relatively large flume size and also the availability of presented data. The test of interest was completed in a flume approximately 20 ft wide and 100 ft long, although only the first 60 ft of flume length had channel centerline data presented in the study. The test ran for 160 hrs. Thalweg traces were presented for the initial channel, after 35 hrs, after 83 hrs, and after the 160 hr duration.

The data inputs that need to be specified for the SRH-Meander model which reflect physical properties of the river system and affect meandering and migration are flow data, channel geometry (planform, profile, and cross-section), channel roughness, bed material size, and bank erosion rates.

The USACOE study reported a range of flows between 0.05 and 0.5 cfs, but it not specify the exact flow rates used in the particular case simulated here. Therefore, during the calibration, the flow rate was adjusted to achieve good agreement between the SRH-Meander output and the USACOE flume study results. It is found that the flow rate of 0.5 cfs gives the best results as of channel alignment and channel bed erosion.

The initial conditions were given in the report for the profile and cross-sectional geometry inputs. Namely, a bed slope of 0.007 ft/ft and a trapezoidal cross-section with a 1.62 ft bottom-width, a 0.23 ft channel height, and a 1.82 ft channel

top-width. The lab data shows that the channel widens during the no sediment feeding condition. The calibration process assumes a constant channel width. A channel bottom-width of 3 ft was used in the calibration since the model cannot determine the channel width change as a priori. The initial channel centerline was also given in the study.

The study reported changes in planform geometry, cross-sectional geometry, and profile geometry during the test. The SRH-Meander model does not allow for dynamic changes of cross-sectional geometry. Thus, geometric parameters were modified during the calibration process.

No estimate for channel roughness was provided in the study. Channel roughness could have been estimated based solely on grain size, however with the channel being small relative to prototype channels, the effects of grain roughness may be more pronounced, perhaps leading to a higher roughness coefficient than would be calculated using typical design equations. Thus, the Manning roughness coefficient was treated as a parameter which was adjusted during model calibration. The alluvium used as the bed and banks of the USACOE study was reported in the form of two grain size distributions: a fine sand ($d_{50} \sim 0.2$mm) made up 80% of the channel material and a silt ($d_{50} \sim 0.045$mm) made up 20% of the channel material.

The bank erosion coefficients were treated as input parameters and adjusted during the calibration process. The SRH-Meander model uses polygons from ArcMap to spatially identify locations and associated erosion rates. Various erosion rates could be assigned at different sections of the channel, but the bed and bank material was essentially uniform throughout the test section and it was expected that a single erosion coefficient for the entire channel should be identifiable. The one exception is at the flume entrance. The USACOE used non-erosive material at the entrance bend, so a polygon encompassing the entrance bend was given an erosion coefficient of approximately zero, and a second polygon was used for the portion of the channel that was allowed to meander. The erosion coefficient associated with the meander polygon was adjusted during the calibration process.

The laboratory study shows that the bank erosion in the upstream bend stopped after the channel bed was eroded and the slope was decreased. The flattening of the slope reduces the velocity and the shear stress to erode the banks. The

deepening of the channel increases the bank resistance to the bank erosion. A unique feasture of SRH-Meander is that it is able to update the terrain elevation, and thus update the channel slope. The raster elevation is updated by considering the mass balance between channel erosion/deposition, incoming sediment rate, outgoing sediment rate, and bank erosion/deposition. Another bank height resistance coefficient is introduced to reduce the erosion of high banks. It is assumed that the bank erosion rate was linearly related to the deviation in velocity from the mean velocity and the resistance force is linearly related to the dimensionless bank height:

$$E_b = (E_0 - Bh/H)u_b \qquad (7.1)$$

where:

E_b = rate of bank erosion [L/T];

E_0 = bank erosion constant [-];

B = resistance coefficient [-];

h = bank height [L];

H = cross sectional water depth [L]; and

u_b = deviation from mean velocity at bank [L/T];

parameters that were changed during calibration for the lab study were the model grid spacing, the channel width, the Manning roughness coefficient, and the erosion coefficient and bank height resistance coefficient for the polygon encompassing the meandering portion of the channel. The model calibration was an iterative process. The calibration parameters were assigned values, the simulation performed, and the results observed. Based on observed results, the calibration coefficients would be adjusted and the model run again to observe changes in the goodness-of-fit between the predicted alignment of the channel based on the SRH-Meander model and the ending channel alignment from the USACOE physical test.

Figure 7.1 shows the thalweg trace after 160 hours with and without mass balance considered and terrain elevation updated. It is shown that the model can predict the non-uniform development of the bends. The bends increased in size from upstream to downstream. During the no sediment feeding condition at the entrance, the channel deepened at the upstream. The upstream channel slope became so flat that the flow no longer had enough velocity and shear stress to erode the bank. Additionally, the upstream channel bank height was increased

due to channel erosion, and the bank was more resistant to the bank erosion. However, the model did not predict the channel phase correctly when compared with bends observed from the laboratory test. When the end of the channel is calibrated to the laboratory data, the first, second, and third bends are all shifted to downstream.
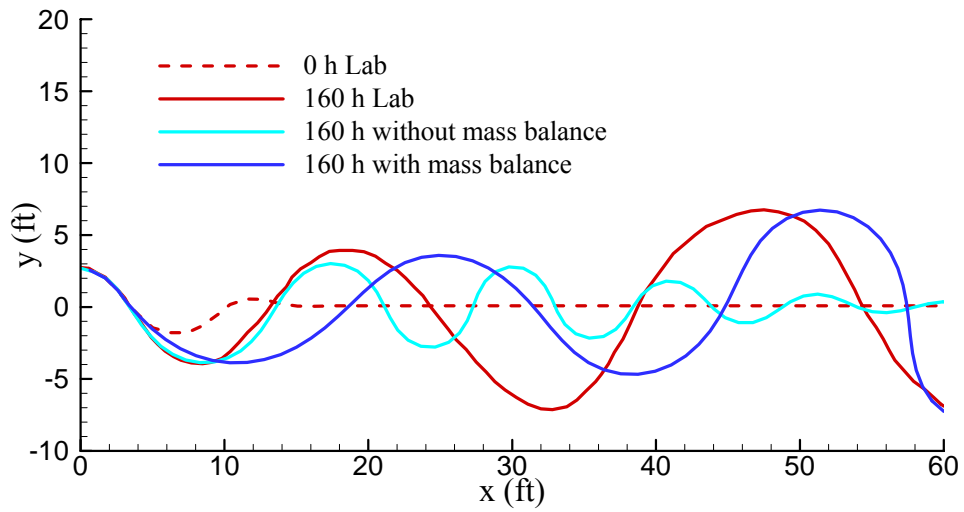

Figure 7.1. Calibration resulting with raster elevation update and bank height resistance coefficient
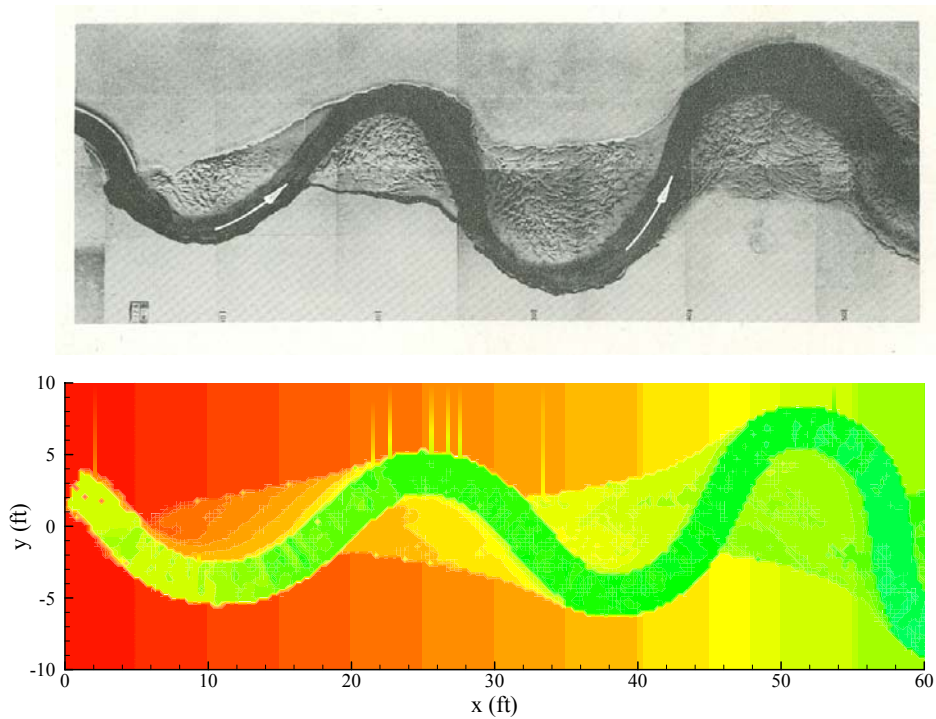
Figure 7.2. Comparison of Channel Profiles

Figure 7.2 visually compares the terrain topography after 160 hours with the photograph taken in the laboratory test. While there were no records of the terrain elevation, it is shown that the model has the potential capacity to predict the floodplain topography after channel migration.

7.2 Model Application to RM 110 of the Middle Rio Grande at RM 110

SRH-Meander was used to simulate the bank migration of the Middle Rio Grande at RM 110. The 1.5 mile reach from Agg/Deg 1247 to Agg/Deg 1262 experienced extensive channel migrations in recent years, and further channel migration of the western bend will endanger the levee and low flow conveyance channel on the west side (Massong, 2006). This example applied SRH-Meander to reproduce the channel migration from 2001 to 2006 by model calibration.

The United States Geological Survey's (USGS) National Water Information System (NWIS) interactive database (http://waterdata.usgs.gov/nwis/) was used as the source for the flow data. Specifically, gage #08354900 at San Acacia was used and the period of daily flows considered was from 01/01/2001 to 12/31/2005. The hydrograph shows that flood from middle April to early July of 2005 reached a peak value of 5980 cfs.

Profile and cross-sectional geometry information was taken from a Reclamation's 2001 HEC-RAS geometry. Channel geometry data consisted of photogrammetric cross sections from aerial photography in 2001. The aerial photography does not include the underwater portion of the channel, only the water surface. The geometry below the water surface was constructed by calculating the rectangular channel that would convey the measured flow rate at the observed water surface elevation.

The model assumes that there was no significant profile and cross-sectional geometry changes during the simulated period. Constant values averaged from HEC-RAS geometry file were used for bank height, floodplain width, channel width, and bank angles. They are 12 ft, 500 ft, 148 ft, and 50°, respectively. The Manning's coefficients used are 0.02 and 0.1 for main channel and floodplain, respectively. Aerial photographs and GIS maps for a range of years for the

Middle Rio Grande were obtained from digitized information in the Rio Grande GIS database (Oliver, 2006).

Information on bed material size was gathered from the SRH-1D model (Holmquist-Johnson, 2005) and used as input. Reclamation performed the flow and sediment transport simulation of the Rio Grande from San Acacia Diversion Dam to Elephant Butte Reservoir with SRH-1D model.

The model calibrates erosion rates to obtain the best results compared with field data. The calibration of the erosion rates were based on the bank material properties that resist the channel erosion. The erosion rates are calibrated values related to the erosion resisting properties of the bank, such as riparian vegetation, large woody debris, cohesive soils, and bank armoring.

The numerical model simulated three bends at RM 110 for a period from 01/01/2001 to 12/31/2005. This period includes the 2005 flood when two bends at RM 110 experienced extensive channel migration. Aerial photographs are available at 2001 and 2006 to calibrate the model. The studied reach spans approximately 1.5 miles from Agg/Deg 1247 to Agg/Deg 1262, downstream of the San Acacia Diversion Dam.

The channel alignment was described by channel thalweg lines. The GIS map contains information about the 'active' channel (Oliver, 2006). A GIS polyline shapefile was created to represent the channel thalweg. A GIS point shapefile was also created. The polyline was divided into equal space points and saved into the newly created point shapefile. Figure 7.3 presents the channel alignments in 2001 and 2006, respectively. The 2006 channel alignment was used for model calibration.
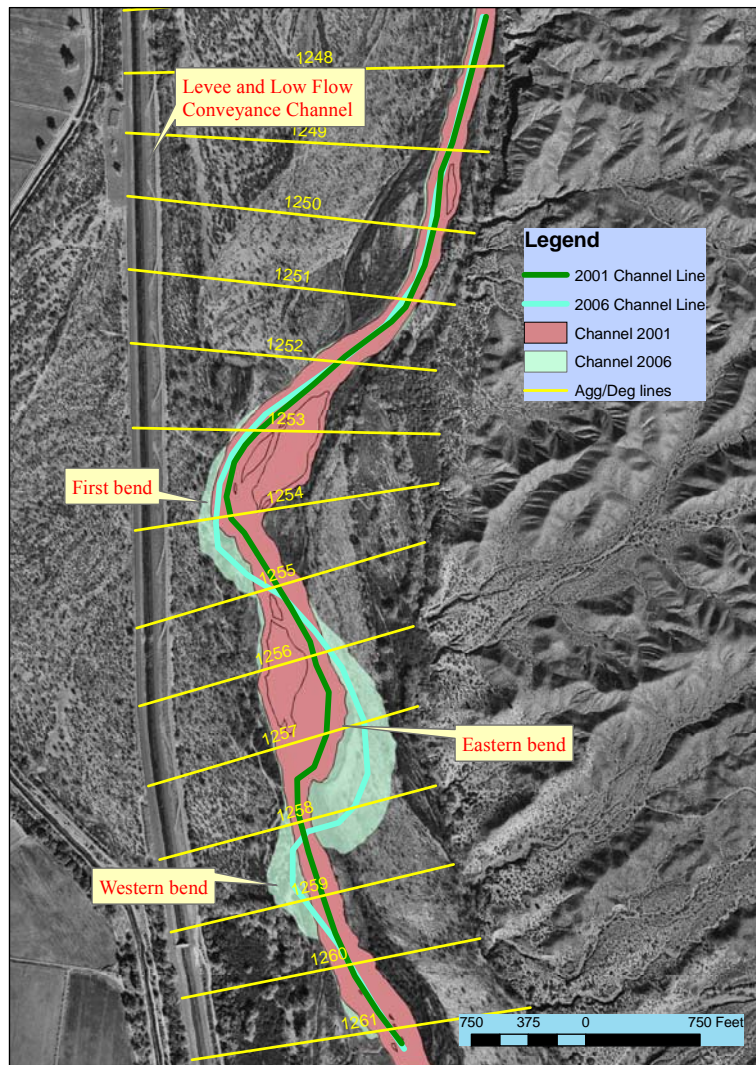
Figure 7.3. Active channels and channel alignments with 2001 aerial photo.

A valley axis for the 2001 channel was digitized (seen in Figure 7.4). The valley axis passes stations where channel locations are nearly fixed and there were no major channel migrations. The valley axis is used to update the channel slope and determine the possible locations of channel cutoffs. The channel is described as left channel and right channel divided by the valley axis. The channel slope is calculated as the average slope in each section of the left channel or right channel. The ratio between left or right channel length to valley axis length is used to determine if a channel cutoff would occur. When the ratio of the length of the channel to the length of the valley exceeds the cutoff ratio, a cutoff occurs. No channel cutoff occurred in this simulated reach.

A polygon shapefile was used to assign erosion coefficients. Areas in the left and right channels are placed into different polygon. Areas with heavy vegetation are included into several polygons, and areas with sparse vegetation are included into several polygons. A total of 32 polygons were created in this model to represent the resisting properties of the channel bank as shown in Figure 7.4.
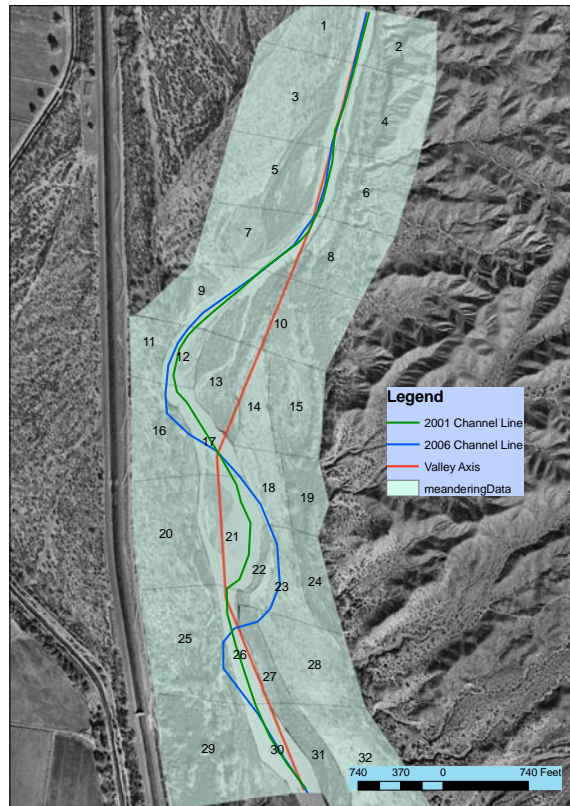

Figure 7.4. Polygons used for assigning erosion coefficients

The model calibration is an iterative process. SRH-Meander displays the simulated channel alignment along with the initial and final channel alignments to help virtually determine the goodness of the calibration. Erosion rate coefficients are major calibration parameters.

Figure 7.5 displays the channel alignments of 2001 and 2006, and the model output nodes representing the simulated channel alignment. The model was calibrated moderately well to final channel alignment. Table 7.1 shows the calibrated erosion rate coefficients corresponding to polygons in Figure 7.4.

The model captures the downstream migration of the upstream bend (shown in Figure 7.5 as first bend). However, more information would be necessary to

determine why the modeled bend has not eroded toward the levee and low flow conveyance channel.

The eastern bend is eroding through two types of surfaces: recently deposited riverine sediments on an active floodplain, with high bank resisting force due to heavy vegetation; and abandoned/terraced riverine sediments on a tall terrace, with less bank resisting force due to sparse vegetation (Massong, 2006). The river is easily eroding the sparsely vegetated tall terrace, as in polygons 18, 19, 23, and 24. The heavily vegetation floodplain, as in polygons 22 and 27, slowed the erosion rate there and created a 'hook' feature at the downstream end of the eastern band. The model reproduced the eastern bend erosion fairly well.

SRH-Meander reproduced the emergence of the western bend. The western bend is a secondary bend which is controlled by the eastern bend. The model results indicate that the western bend is also migrating downstream, which is also seen in the field.
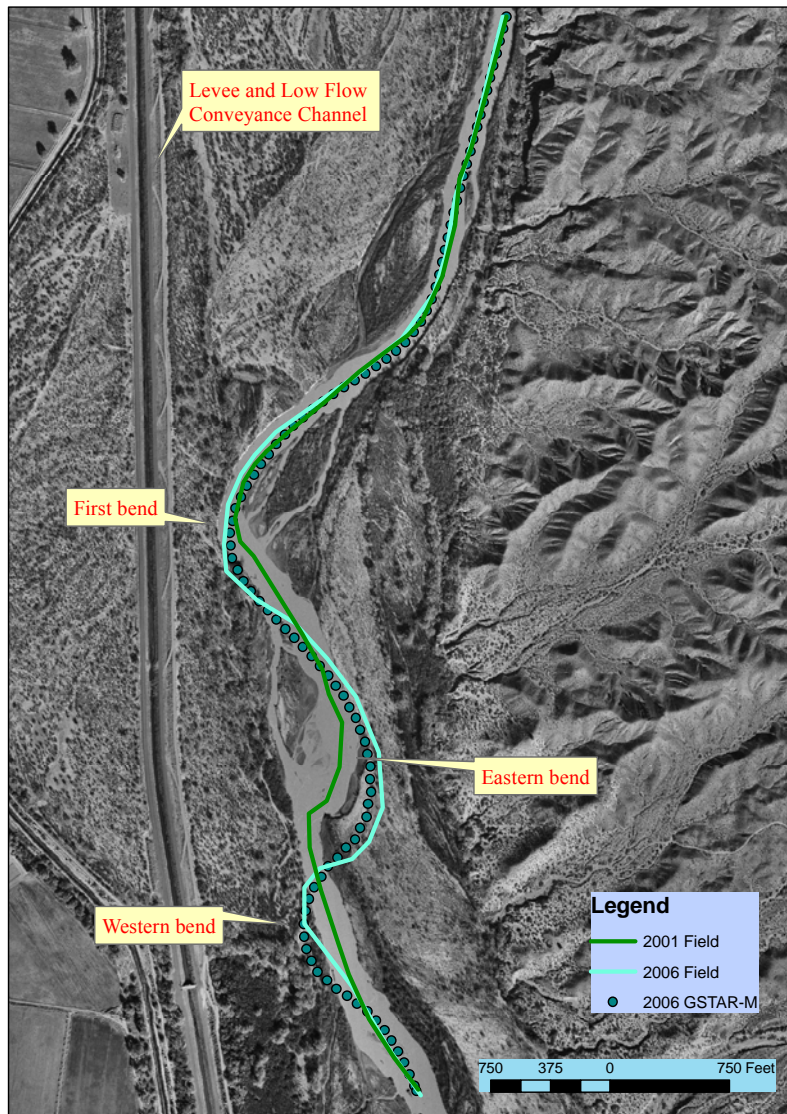
Figure 7.5. Calibration reach results.

Table 7.1 Calibrated erosion rate

Polygon	Erosion Rate	Polygon	Erosion Rate
1	1.00E-05	17	5.00E-05
2	1.00E-05	18	1.00E-04
3	1.00E-05	19	1.00E-04
4	1.00E-05	20	3.00E-04
5	1.00E-05	21	3.00E-04
6	1.00E-05	22	8.00E-05
7	1.00E-05	23	4.00E-04
8	1.00E-05	24	4.00E-04
9	1.00E-05	25	1.00E-04
10	1.00E-05	26	1.00E-04
11	1.00E-05	27	1.00E-05
12	1.00E-05	28	4.00E-04
13	1.00E-05	29	1.00E-05
14	1.00E-05	30	1.00E-05
15	1.00E-05	31	1.00E-05
16	1.00E-05	32	1.00E-05

7.3 Model Application to the Sacramento River.

A portion of the Middle Sacramento from river miles 218.5 to 206.5 was also simulated. Figure 7.6 presents the locations of the studied reach downstream of Red Bluff, California. The application considered the span of time from 1976 to 1999. The data collected and used for the calibration of the middle Sacramento River is described below, but in general, the source and quality of data will vary for each project and vary the results.

Figure 7.6. Reach used for model calibration (RM 218.5-RM206.5).

The United States Geological Survey's (USGS) National Water Information System (NWIS) interactive database (http://waterdata.usgs.gov/nwis/) was used as the source for the flow data. Specifically, gage #11377100 was used and the period of daily flows considered was from 10/01/76 to 09/30/99.

Profile and cross-sectional geometry information was taken from a United States Corps of Engineers publication, "Sacramento and San Joaquin River Basins, Comprehensive Study" (U.S. Army Corps of Engineers, 2002). This study produced a HEC-RAS geometry model of the river that was used in this study. From this study information on channel roughness and bed material size were gathered and used as input to the model. The river planform geometry

information was made available by the State of California Department of Water Resources (DWR). Aerial photographs and GIS maps for a range of years for the Sacramento River were provided by the DWR.

The bank erosion coefficient were adjusted during the calibration process. The results from the model calibration could be compared to existing field data, such as surface geology, vegetation, land use, channel bank information, levee location, and riprap linings, etc.

Table 7.2 presents a summary of the parameters – both calibration parameters as well as those determined before calibration – used during calibration of the SRH-Meander model to the Sacramento River. All of the erosion coefficients are not listed, but rather the minimum, average, and maximum values are presented. Figure 7.7 displays the centerlines for the 1976, 1981, 1991, and 1999 channels, respectively, and the SRH-Meander output nodes representing the model output channel centerlines in corresponding years.

Table 7.2. Summary of parameters used during SRH-Meander model calibration

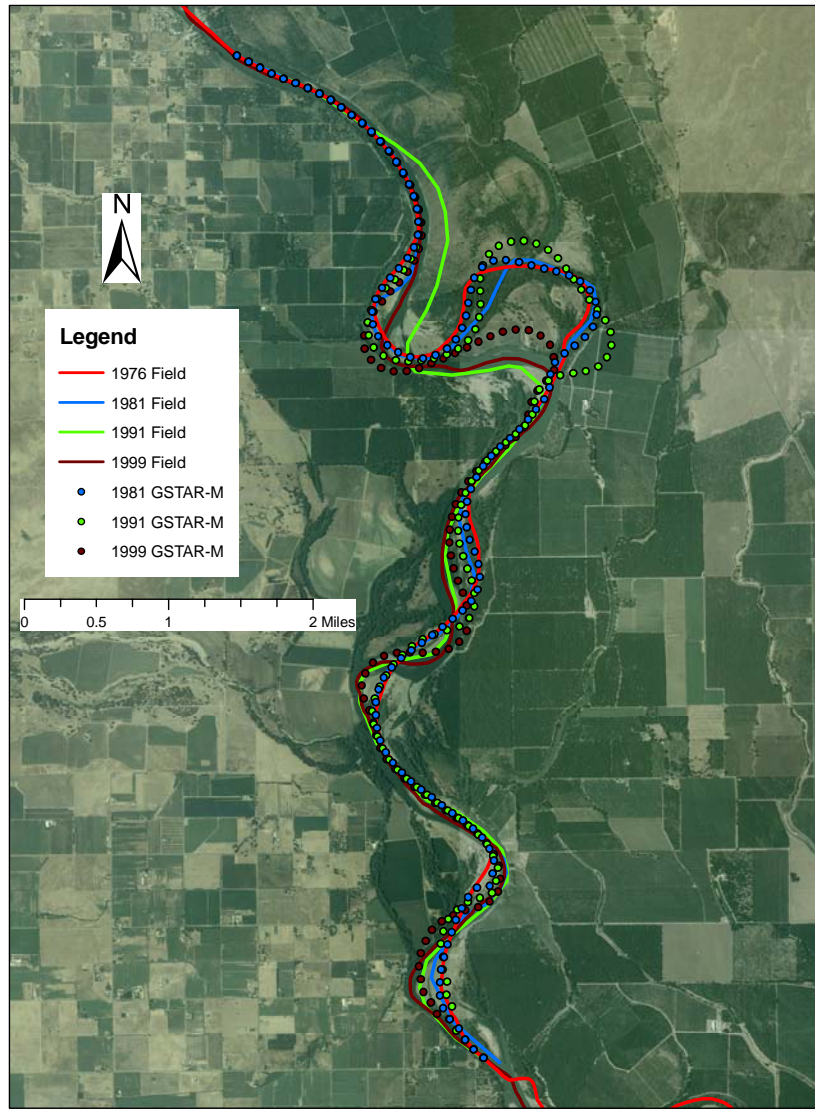|		
Pre-determined parameters	Ave. Channel Width (ft)	789
	Manning n (-)	0.032
	Ave. Energy Slope (ft/ft)	0.00048
	Bed Material Size (mm)	14
	Number of Polygons	47.00
Calibration parameters	Grid Spacing (-)	0.6
	Cutoff Ratio (-)	3.8
	Min. Erosion Coefficient (-)	8.90E-09
	Ave. Erosion Coefficient (-)	5.05E-05
	Max. Erosion Coefficient (-)	1.80E-04

Figure 7.7. Calibration results

The model calibration is considered to be reasonable, but some discrepancies still exist. The average absolute distance of the simulated channel coordinates to the actual 1999 channel centerline was 76 feet. These values are small relative to the average channel top widths of approximately 800 feet for this reach. The value of 0.60 for the grid spacing agrees with the finding of Crosato (2007) numerical meander models that the "optimal distance between successive grid points had the order of half the channel width".

In general, the SRH-Meander was better at modeling changes in bend amplitude than at modeling bend translation (Figure 7.7). Whether the model predicts

translation versus amplification is primarily a function of the channel roughness input parameter combined with the calculated curvature of the centerline. The roughness parameter can only have a single value for the entire model and for the full range of flows used, which may not reflect the actual channel. Calibrating one bend with a given curvature to amplify properly may cause a subsequent bend of similar curvature to not translate as was observed.

Channel cutoff was predicted for one bend (Figure 7.7). SRH-Meander simulates the channel cutoffs when the ratio of the length of channel to the length of the valley exceeds a threshold value input by the user. When the channel sinuosity exceeds a limit, the channel has not enough energy to carry the incoming flow and sediment, and the river abandons an existing portion of its length to find a new shorter and steeper path. A straight line is used to link the two points of the channel during the cutoff. After the cutoff, points are redistributed along the channel at equal distances. The model calibration tried to match the simulated channel profile with 1999 field data. While the model reproduced the channel profile in 1999, the model reproduced the channel cutoff before 1991 and the field data shows that the cutoff occurred after 1991.

Another capability of SRH-Meander is to calculate the terrain elevation changes after the channel migration. Figure 7.8 shows the terrain elevation for the initial year 1999 when the field data is available. Figure 7.9 shows the predicted terrain elevation in 2019. Elevation data are only available in 1999 and no other data is available to determine the accuracy of SRH-Meander in predicting terrain elevation revision due to channel migration. Figure 7.10 shows the predicted terrain change from 1999 to 2019, which displays the erosion (red) near the outside of the bend and deposition (green) near the inside of the bend. The black polygon shows the total area that the channel would have swapped in the 20 year period. Accurate prediction of terrain elevation change is helpful to determine the area targeted for vegetation establishment.
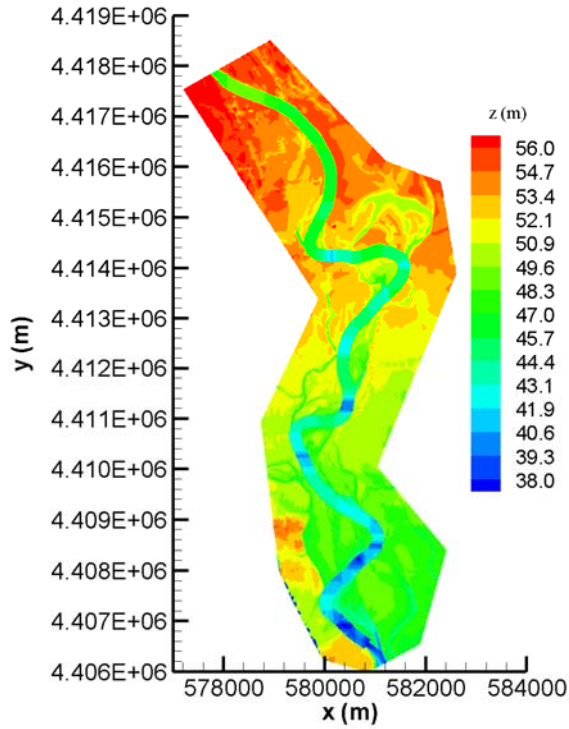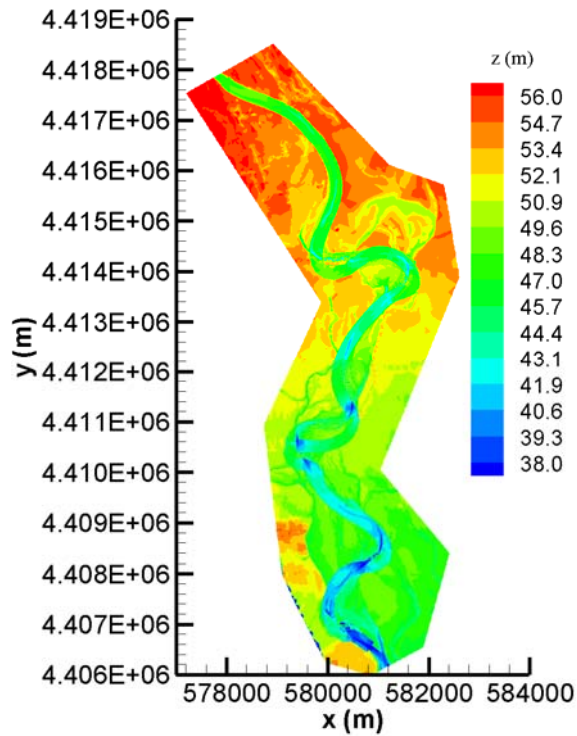
Figure 7.8. Calculated terrain elevation in 1999
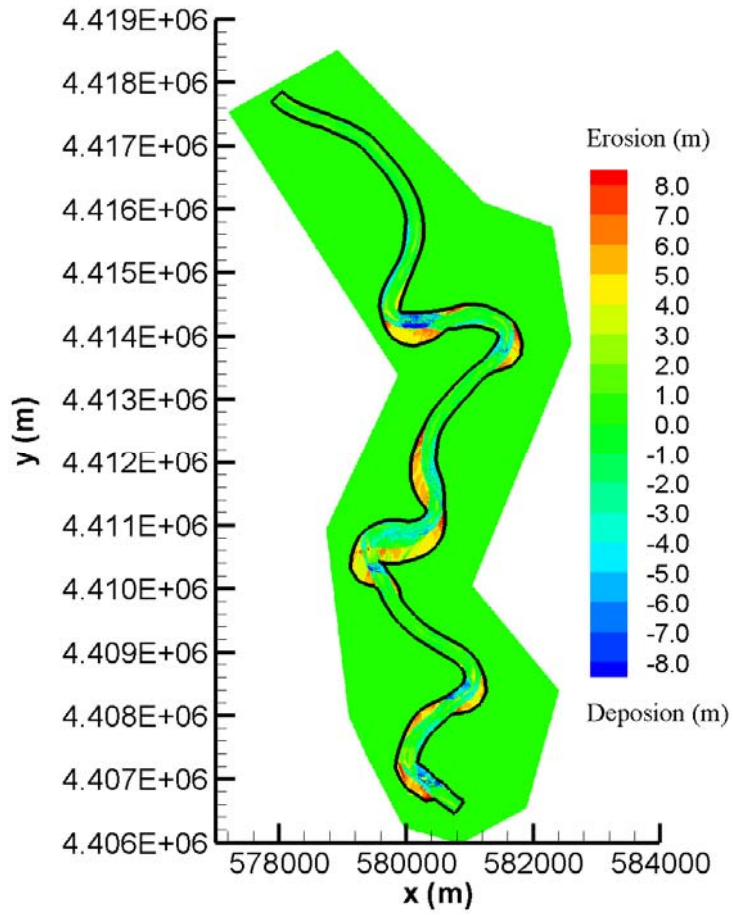

Figure 7.9. Calculated terrain elevation in 2019

Figure 7.10. Calculated terrain elevation change from 1999 to 2019

REFERENCES

Brunner, G.W. (2001). *HEC-RAS River Analysis System, Version 3.0*, Hydrologic Engineering Center, US Army Corps of Engineers, Davis, CA 95616.

Camporeale, C., Perona, P., Porporato, A., and RIdolfi, L. (2005). "On the Long-term Behavior of Meandering Rivers," *Water Resource Research*, Vol. 41, 1-13.

Crosato, A. (2007). "Effects of smoothing and regridding in numerical meander migration models", Water Resources Research, VOL. 43, W01401, doi:10.1029/2006WR005087.

Edwards, B.F. and Smith, D.H (2002). "River Meandering Dynamics," *Physical Review E*, Vol. 65, DOI: 10.1103/PhysRevE.65.046303

Engelund, F. (1974). "Flow and Bed Topography in Channel Bends," *ASCE Journal Hydraulics Division*, Vol. 100(11), 1631-1648.

Han, Q. (1980). "A study on the non-equilibrium transportation of suspended load," Proc. of the Int. Symp. on River Sedimentation, Beijing, China, pp. 793–802. (In Chinese.)

Haswegawa, K. (1989). "Studies on Qualitative and Quantitative Prediction of Meander Channel Shift," in *Water Resources Monograph No. 12: River Meandering*, edited by S. Ikeda and G. Parker, American Geophysical Union, Washington DC, 215-235.

Holmquist-Johnson, C.L. (2005), "Sediment Model for the Middle Rio Grande – Phase 1, San Acacia Diversion Dam to Elephant Butte Reservoir", Bureau of Reclamation, Technical Service Center, Sedimentation and River Hydraulics Group, Denver, CO.

Howard, A.D. (1995). "Documentation for Meander Flow, Bank Erosion and Floodplain Deposition Program," University of Virginia.

Ikeda, S. G., Parker, G., and Sawai, K. (1981). "Bend theory of river meanders: 1. Linear development", Journal of Fluid Mechanics, Vol. 112, 363–377.

Jain, S.C. (2000). *Open Channel Flow*, John Wiley & Sons, Inc.

Johannesson, H., and Parker, G. (1989). "Linear Theory of River Meanders," in *Water Resources Monograph No. 12: River Meandering*, edited by S. Ikeda and G. Parker, American Geophysical Union, Washington DC, 181-213.

Lancaster, S.T. (1998). *A Nonlinear River Meandering Model and its Incorportaion in a Landscape Evolution Model*, Ph.D. Thesis, Massachusetts Institute of Technology.

Larsen, E. W. (1995). *Mechanics and Modeling of River Meander Migration*, Ph.D. Thesis, University of California at Berkeley.

Larsen, E., Anderson, E., Avery, E, and Dole, K. (2002). *The controls on and evolution of channel morphology of the Sacramento River: A case study of River Miles 201-185*, Geology Department, University of California, Davis, California.

Massong, T. (2006). *Evolution of the Bends at RM 110*, Technical Report, Bureau of Reclamation, Environment Division, Albuquerque Area Office, Upper Colorado Region.

Meyer-Peter, E., and Muller, R. (1948). "Formula for bed-load transport," Proc. of the Int. Assoc. for Hydraulic Research, 2nd Meeting, Stockholm.

Nanson, G. C. and Hickin, E. J. (1986). "A Statistical Analysis of Bank Erosion and Channel Migration in Western Canada," *Geological Society of America Bulletin*. Vol.97, 497-504.

Nelson, J. and Smith, J.D. (1989). "Flow in Meandering Channels with Natural Topography," in *Water Resources Monograph No. 12: River Meandering*, edited by S. Ikeda and G. Parker, American Geophysical Union, Washington DC, 69-102.

Oliver, J. (2006). Personal Communications.

Parker, G. and Johannesson, H. (1989). "Observations on Several Recent Theories of Resonance and Overdeepening in Meandering Channels," in *Water Resources Monograph No. 12: River Meandering*, edited by S. Ikeda and G. Parker, American Geophysical Union, Washington DC, 379-415.

Press, W.H., Teukolsky, S.A., Vetterling, W.T., and Flannery, B.P. (1992). *Numerical Recipes in Fortran, The Art of Scientific Computing*, Second Edition, Cambridge University Press.

Randle, T.J. (2004). "Channel Migration Model for Meandering Rivers," a thesis submitted to the University of Colorado at Denver in partial fulfillment of the requirements for the degree of Masters of Science Civil Engineering.

Seminara, G., Zolezzi, G., Turbino, M., and Zardi, D. (2001). "Downstream and Upstream Influence in River Meandering. Part 1. Planimetric Development," *Journal of Fluid Mechanics*, Vol. 438. 213-230.

Sun, T., Meakin, P., and Jøssang, T. (2001a). "A computer model for meandering rivers with multiple bed load sediment sizes, I. Theory," *Water Resources Research*, Vol.37(8), 2227-2241.

Sun, T., Meakin, P., and Jøssang, T. (2001b). "A computer model for meandering rivers with multiple bed load sediment sizes, II. Computer simulations," *Water Resources Research*, Vol.37(8), 2243-2258.

Thomas, J.L. (1998). *Predicting Meander Migration of the Sacramento River, CA: Comparison of Empirical and Physically-based mathematical Modeling Approaches*, Master's Thesis, Civil and Environmental Engineering, University of California at Davis.

U.S. Army Corps of Engineers (1945). *A Laboratory Study of the Meandering of*

Alluvial Rivers U.S. Waterways Experiment Station, Vicksburg, MS.

U.S. Army Corps of Engineers (2002). "Sacramento and San Joaquin River Basins, California, Comprehensive Study, Technical Studies Documentation", US Army Corp of Engineers, Sacramento District, December 2002.

Yang, C. T. and Song, C. C. (1979). "Theory of minimum rate of energy dissipation," *ASCE Journal of the Hydraulics Division*, Vol. 105(7), 769-784.

Yang, C.T. (1973). "Incipient motion and sediment transport," *ASCE Journal of Hydraulic Division,* Vol. 99(10), 1679-1704.

Yang, C.T. (1984). "Unit stream power equation for gravel," *ASCE Journal of Hydraulic Division,* Vol. 110(12)1783-1797.

Zolezzi, G., and Seminara, G. (2001). "Downstream and Upstream Influence in River Meandering. Part 1. General Theory and Application to Overdeepening," *Journal of Fluid Mechanics*, Vol. 438. 183-211.